

# A Grey-box Attack against Latent Diffusion Model-based Image Editing by Posterior Collapse

Zhongliang Guo<sup>1</sup>, Lei Fang<sup>1</sup>, Jingyu Lin<sup>2</sup>, Yifei Qian<sup>1</sup>, Shuai Zhao<sup>3</sup>, Zeyu Wang<sup>4</sup>, Junhao Dong<sup>3</sup>, Cunjian Chen<sup>2</sup>, Ognjen Arandjelović<sup>1</sup>, Chun Pong Lau<sup>5</sup>

<sup>1</sup>University of St Andrews

<sup>2</sup>Monash University

<sup>3</sup>Nanyang Technological University

<sup>4</sup>Zhejiang University

<sup>5</sup>City University of Hong Kong

{zg34,lf28,yq1,oa7}@st-andrews.ac.uk, {jingyu.lin,cunjian.chen}@monash.edu, {shuai.zhao,junhao003}@ntu.edu.sg, wangzeyu2020@zju.edu.cn, cplau27@cityu.edu.hk

## Abstract

Recent advancements in generative AI, particularly Latent Diffusion Models (LDMs), have revolutionized image synthesis and manipulation. However, these generative techniques raises concerns about data misappropriation and intellectual property infringement. Adversarial attacks on machine learning models have been extensively studied, and a well-established body of research has extended these techniques as a benign metric to prevent the underlying misuse of generative AI. Current approaches to safeguarding images from manipulation by LDMs are limited by their reliance on model-specific knowledge and their inability to significantly degrade semantic quality of generated images. In response to these shortcomings, we propose the Posterior Collapse Attack (PCA) based on the observation that VAEs suffer from posterior collapse during training. Our method minimizes dependence on the white-box information of target models to get rid of the implicit reliance on model-specific knowledge. By accessing merely a small amount of LDM parameters, in specific merely the VAE encoder of LDMs, our method causes a substantial semantic collapse in generation quality, particularly in perceptual consistency, and demonstrates strong transferability across various model architectures. Experimental results show that PCA achieves superior perturbation effects on image generation of LDMs with lower runtime and VRAM. Our method outperforms existing techniques, offering a more robust and generalizable solution that is helpful in alleviating the socio-technical challenges posed by the rapidly evolving landscape of generative AI.

## Introduction

The field of generative artificial intelligence has witnessed unprecedented advancements, particularly in the domain of image synthesis and manipulation. State-of-the-art methodologies, exemplified by diffusion models such as Stable Diffusion (Rombach et al. 2022), have demonstrated remarkable capabilities in producing photorealistic imagery with exceptional fidelity and diversity. These technological breakthroughs have not only revolutionized creative indus-

tries but have also democratized access to sophisticated image editing tools, empowering users across various domains.

However, the proliferation of such powerful technologies inevitably engenders a concomitant set of ethical quandaries and potential security vulnerabilities. Of particular concern is the prospect of data misappropriation and intellectual property infringement. The facility with which diffusion-based models can be employed to manipulate existing visual content presents a significant challenge to the integrity of digital assets. For instance, malicious actors could exploit Stable Diffusion to edit copyrighted images, effectively “laundering” them by removing or altering identifying features (Rombach et al. 2022). This process of “de-copyrighting” not only undermines the rights of content creators but also poses a threat to the economic ecosystems built around digital imagery, potentially destabilizing industries ranging from photography to digital art.

In the realm of machine learning security, adversarial attacks have emerged as a critical area of study (Lau et al. 2023a). These attacks aim to perturb the input of machine learning models in ways that are imperceptible to humans but can significantly disrupt the model’s output. Interestingly, this concept of adversarial attacks provides a potential solution to the misuse of generative AI. By introducing carefully crafted, acceptable perturbations to data that could be misused, it may be possible to impede the ability of diffusion models to edit or manipulate such content effectively.

Current protection techniques often rely heavily on extensive prior knowledge, specifically requiring full white-box access to the parameters of the target models (Liang et al. 2023; Salman et al. 2023; Liang and Wu 2023; Xue et al. 2024). This assumption is largely impractical in real-world scenarios, especially given the rapid pace of technological advancement in generative AI. The proliferation of model architectures and constant iterations of backbone networks create a dynamic landscape where protection methods quickly become obsolete. Developing a universal method that can effectively protect against the vast majority of generative models without detailed knowledge of their internal structures is exceedingly difficult. Furthermore, the diversity of model architectures means that a method designed for

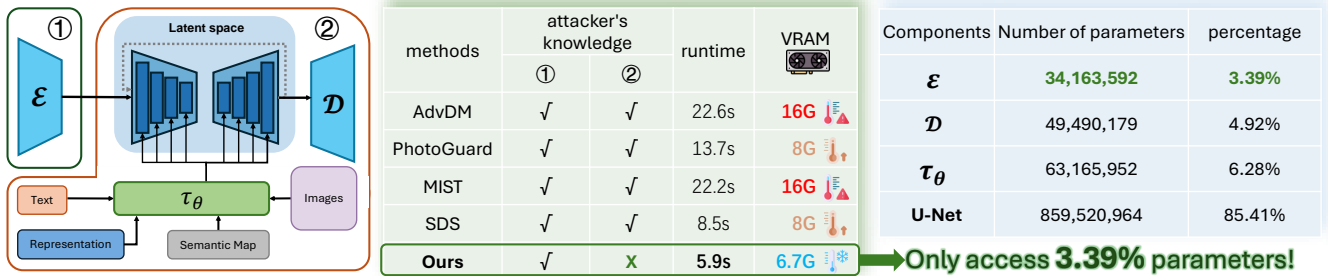


Figure 1: Comparison of our proposed method with AdvDM (Liang et al. 2023), PhotoGuard (Salman et al. 2023), MIST (Liang and Wu 2023), and SDS (Xue et al. 2024). Our method only requires access to the encoder of the VAE, achieving equal or superior performance on multi scenarios (Figure 2) with comparable image editing semantic degrade, lower runtime, and less occupied VRAM.

one particular model or family may be entirely ineffective against others. This lack of generalizability severely limits the practical applicability of such approaches in a rapidly changing technological environment.

Secondly, while existing approaches successfully prevent infringer-desired alterations and introduce visible watermark-like artifacts in post-editing images as indicators of unauthorized manipulation (Liang et al. 2023; Xue et al. 2024), these approaches fail to comprehensively disrupt the semantic quality of generation as edited adversarial samples still remain the perceptual integrity with original clean image. Consequently, these methods struggle to achieve the goal of thoroughly degrading the semantic quality of manipulated outputs.

Given these limitations in current protective measures and the narrow scope of existing attack methods on diffusion models, addressing these critical gaps in the field requires a solution that meets several key criteria:

- To ensure broader applicability and resilience against rapid technological advancements, the method should minimize dependence on white-box information of the target models or merely rely on white-box information that is public across the most popular current methods.
- The method should cause significant degradation to the semantic generation quality of the most popular image editing and generation methods within the bounds of human visual sensitivity.
- The method should exhibit strong transferability, easily generalizing across various models and architectures.

In light of these challenges, we aim to propose a new protection method targeting Variational Autoencoders (VAEs) hinge on a key observation: the vast majority of state-of-the-art generative models leveraging VAEs, where VAEs perform as an upstream bottleneck. This commonality presents a promising opportunity to design a more universal attack strategy targeting the LDMs, potentially addressing the need for a generalizable protection method.

In literature, existing attacks on VAEs primarily focus on corrupting the decoding process to lead to deteriorated reconstruction (Kuzina, Welling, and Tomczak 2022), which does not align with our objective of perturbing downstream

diffusion process. Notably, the encoding posterior distribution of VAEs, often overlooked in previous attack methods, provides a more comprehensive representation of the latent space, which is the bottleneck of all downstream tasks, potentially leading to more effective and generalizable attacks.

Drawing inspiration from the phenomenon of posterior collapse in VAEs’ training (Razavi et al. 2019), where the latent variables fail to capture meaningful information about the input data, we suggest to intentionally induce this collapse as an attack strategy. Thus, we propose Posterior Collapse Attack (PCA), inducing collapse in the posterior distribution with our proposed new loss function, resulting worse semantic quality of edited image. As illustrated in Figure 1 and 2, our method effectively perturbs downstream LDMs in a near black-box manner (only 3.39% parameters). This approach not only aligns with our goal of disrupting downstream tasks but also offers a more robust and transferable solution. Unlike previous methods that rely heavily on model-specific knowledge, our method merely leverages encoder of VAEs, providing a more universally applicable protection mechanism against unauthorized image manipulation across various generative AI architectures.

Our contributions can be summarized as follows:

- We introduce the Posterior Collapse Attack that merely exploits the common VAE structure in LDMs, utilizing a novel loss function to cause the posterior collapse. Our method induces a significant semantic collapse of LDM-edited images, with minimal model-specific knowledge and less computational resources.
- Our experimental results demonstrate that PCA, operating with near black-box adversarial information, effectively prevent LDM-based image editing across various architectures and resolutions, outperforming existing methods in terms of transferability and robustness.

## Related Work

### Generation Models

Diffusion Probabilistic Model (DPM) (Ho, Jain, and Abbeel 2020) has achieved state-of-the-art results in density estimation (Kingma et al. 2021) and sample quality (Dhariwal and Nichol 2021). These models are powerful due to

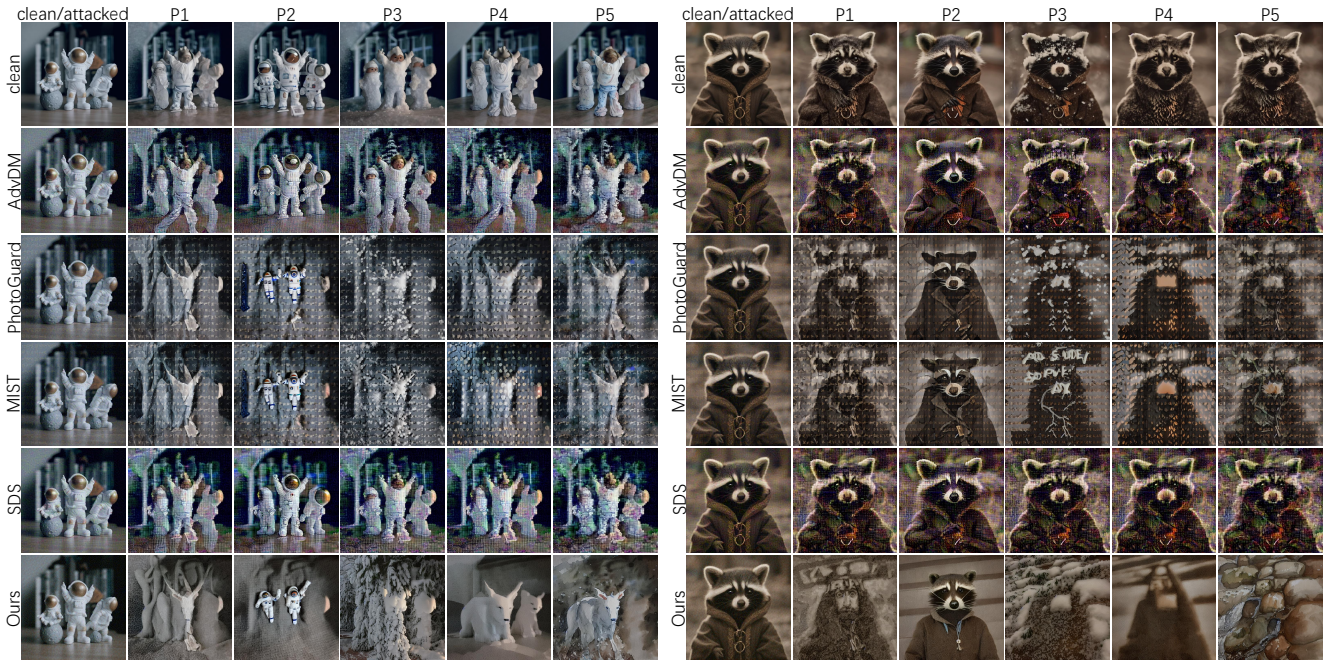


Figure 2: Comparison of our method with other baselines. The first column shows the original images to be manipulated. The top row displays the clean image and its manipulation results, while subsequent rows show attacked images and their corresponding outputs. We apply various prompts to simulate common scenarios: P1 (void text), P2 (BLIP-generated caption: “small toy astronauts standing next to each other” and “a raccoon dressed as lord”), P3 (weather change: “add some snow”), P4 (lighting adjustment: “apply sunset lighting”), and P5 (style transfer: “make it like a watercolor painting”). Our proposed method significantly disrupts image editing, causing substantial semantic loss. This is particularly evident in the results for P1, where the structural information of the edited image without prompt is completely lost.

their U-Net backbone, which suits the inductive biases of image-like data. However, they face challenges in inference speed and training costs, especially for high-resolution images. To address these limitations, researchers have developed approaches like Denoising Diffusion Implicit Models (DDIM) (Song, Meng, and Ermon 2021) to enhance sampling speeds, and explored two-stage processes. Latent Diffusion Models (LDM) (Rombach et al. 2022) use autoencoding models to learn a perceptually similar space with lower computational complexity, while VQ-VAEs (Yan et al. 2021; Razavi, Van den Oord, and Vinyals 2019) and VQGANs (Yu et al. 2022; Esser, Rombach, and Ommer 2021) utilize discretized latent spaces and adversarial objectives to scale to larger images. These advancements aim to overcome the challenges of complex training, data shortages, and computational costs associated with diffusion models, particularly for high-resolution image synthesis.

### Adversarial Attack

The field of adversarial machine learning was catalyzed by the seminal work of Szegedy et al. (2014), who first uncovered the vulnerability of neural networks. Subsequent research has led to the development of various attack methodologies (Goodfellow, Shlens, and Szegedy 2015; Madry et al. 2018). The implications of adversarial attacks raised significant concerns in critical applications. This has spurred

the development of defensive strategies, such as adversarial training (Lau et al. 2023b) and input transformation (Lin et al. 2020b). We have seen the expansion of adversarial attack research into more complex domains (Liu et al. 2023; Guo et al. 2024a; Li et al. 2024; Zhao et al. 2024).

**Attack on VAEs.** Adversarial attacks on VAEs have attracted significant research attention. Most existing research on VAE attacks focused on manipulating the input or latent space to affect reconstruction output (Tabacof, Tavares, and Valle 2016; Gondim-Ribeiro, Tabacof, and Valle 2018; Kos, Fischer, and Song 2018; Kuzina, Welling, and Tomczak 2022), aiming to generate adversarial examples that would be reconstructed as images from different classes. Our approach, however, differs significantly from these previous works. We specifically target the disruption of downstream tasks based on VAE encodings, such as diffusion models, rather than the VAEs’ own reconstruction. Furthermore, we attack the parameters of the approximate posterior distribution produced by the encoder, instead of the latent variables themselves. This approach allows us to explore vulnerabilities in VAE-based systems, particularly in scenarios where VAEs serve as feature extractors or in applications relying on the distributional properties of encoded representations.

**Attack on Diffusion-based Image Editing.** Recent research has paid attention to adversarial attacks against diffusion models for image editing. Liang et al. (2023) targeted

the noise prediction module, while Salman et al. (2023) and Shan et al. (2023) minimized latent space distances. Liang and Wu (2023) combined semantic and textural losses for protection. Xue et al. (2024) revealed the encoder’s vulnerability in latent diffusion models and proposed using Score Distillation Sampling to reduce computational costs. However, these approaches often rely heavily on full white-box access to target models or extensive knowledge of fundamental generative model principles. This dependency limits their practical applicability, especially given the rapid evolution of generative AI architectures. There is a need for methods that are less dependent on model-specific knowledge, can significantly degrade generation quality, and exhibit strong transferability across various models. Figure 1 shows the comparison of various methods across attacker’s knowledge of the generative model, runtime, and VRAM.

### Preliminary

Perceptual compression models typically use an autoencoder trained with a perceptual loss (Zhang et al. 2018) and a patch-based (Isola et al. 2017) adversarial objective (Dosovitskiy and Brox 2016). Specifically, given an image  $\mathbf{x} \in \mathbb{R}^{H \times W \times 3}$  in pixel space,  $\mathbf{x}$  is encoded into latent representation  $\mathbf{z} = \mathcal{E}(\mathbf{x}) \in \mathbb{R}^d$  by an autoencoder. A decoder  $\mathcal{D}$  reconstructs the image from the latent, giving  $\tilde{\mathbf{x}} = \mathcal{D}(\mathbf{z}) = \mathcal{D}(\mathcal{E}(\mathbf{x}))$ , where  $\mathbf{x} \in \mathbb{R}^{H \times W \times 3}$ . The encoder downsamples the image by a factor  $f = H/h = W/w$ ,  $f$  is often set as 8 in latent diffusion models.

We focus on VAE, which is used for most of the state-of-the-art LDMs. VAE can be considered as a probabilistic generative extension of the ordinary autoencoders. The encoder of a VAE aims at approximating the intractable posterior distribution of the latent variable  $\mathbf{z}$  by a Gaussian distribution  $q(\mathbf{z}|\mathbf{x}) = \mathcal{N}(\boldsymbol{\mu}, \text{diag}(\boldsymbol{\sigma}^2))$ . The training proceeds by minimizing the KL divergence between the approximating variational distribution  $q(\mathbf{z})$  and the true posterior  $p(\mathbf{z}|\mathbf{x})$ .

The Latent Diffusion Model is one of the most popular image generation or editing methods. During training, an image  $\mathbf{x}_0$  and a condition  $\mathbf{c}$  are used as inputs. The image is encoded into a latent code  $\mathbf{z}_0$  by an image encoder, such as VAE or its variants. This latent code  $\mathbf{z}_0$  is then progressively combined with Gaussian noise  $\epsilon$  through a forward process, which can be summarized as follows:

$$\mathbf{z}_t = \sqrt{\bar{\alpha}_t} \mathbf{z}_0 + \sqrt{1 - \bar{\alpha}_t} \epsilon, \epsilon \sim \mathcal{N}(\mathbf{0}, \mathbf{I}), \quad (1)$$

where  $\bar{\alpha}_t = \prod_{i=1}^t \alpha_i, \alpha_i \in (0, 1)$ .

The diffusion model is trained to approximate the original data distribution with a denoising objective:

$$\mathbb{E}_{\mathbf{z}_0, \mathbf{c}, \epsilon, t} [\|\epsilon_\theta(\mathbf{z}_t, \mathbf{c}, t) - \epsilon\|], \quad (2)$$

where  $\epsilon_\theta$  is the model prediction. During inference, with a random Gaussian noise start  $\mathbf{z}_T$  and condition  $\mathbf{c}$ , the diffusion model carries out the opposite process from step  $T$  down to 1 to get the encoding of sampled image  $\hat{\mathbf{z}}_0$  by:

$$\hat{\mathbf{z}}_{t-1} = \frac{1}{\sqrt{\alpha_t}} \left( \hat{\mathbf{z}}_t - \frac{1 - \alpha_t}{\sqrt{1 - \bar{\alpha}_t}} \epsilon_\theta(\hat{\mathbf{z}}_t, \mathbf{c}, t) \right) + \sigma_t \epsilon, \quad (3)$$

where  $\sigma_t = \frac{1 - \bar{\alpha}_{t-1}}{1 - \bar{\alpha}_t} \beta_t, \beta_t = 1 - \alpha_t$ .

## Method

### Problem Definition

Adversarial attack aims to craft an imperceptible perturbation  $\delta$ , added on the clean image  $\mathbf{x}$  as the adversarial sample  $\mathbf{x}_{adv}$ , resulting in the wrong or disruptive output of machine learning models. The key concept of the adversarial attack against LDM-based image editing can be summarized as two objectives:

$$\begin{aligned} \textbf{Objective 1: } & \min_{\delta} \mathcal{D}(f(\mathbf{x} + \delta), \mathbf{x} + \mathbf{w}) \quad s.t. \|\delta\|_p \leq \epsilon, \\ \textbf{Objective 2: } & \max_{\delta} \mathcal{D}(f(\mathbf{x} + \delta), f(\mathbf{x})) \quad s.t. \|\delta\|_p \leq \epsilon, \end{aligned}$$

where  $f(\cdot)$  is a kind of LDM-based image editing method;  $\mathbf{w}$  refers to a kind of watermark artifact;  $\mathcal{D}(\cdot)$  measures the perceptual distance between two inputs, indicating the visual consistency of two images in human visual perspective;  $\|\cdot\|_p$  means applying a constraint on the vector, in most cases, this serves to maintain the visual integrity of the adversarial sample, following the  $\ell_\infty$  norm. Notably, Objective 1 will cause similar results to Objective 2, i.e., there will be some distance in  $\mathcal{D}$ ’s space between  $f(\mathbf{x} + \delta)$  and  $\mathbf{x}$ .

Existing methods in the literature typically address either Objective 1 or Objective 2. However, both approaches often require extensive white-box information about the target model, particularly access to the neural backbone U-Net of the LDM. This heavy reliance on model-specific details limits their transferability and applicability across different LDM architectures, requiring more computing resource.

Our method focuses primarily on Objective 2, but takes a fundamentally different approach. Instead of relying on detailed knowledge of the entire LDM pipeline, we exploit the inherent characteristics of LDM-based editing by targeting the VAE component, which is common across various LDM architectures. This strategy allows us to achieve the goal of maximizing the disparity between  $f(\mathbf{x}_{adv})$  and  $f(\mathbf{x})$  without requiring extensive access to model-specific information, particularly the compute-intensive and model-specific U-Net component. By concentrating on the VAE, our approach aligns more closely with real-world scenarios where full model access may not be available, providing an efficient solution to prevent infringers from exploiting LDM-based image editing outputs.

### Posterior Collapse

**Variational Autoencoder.** A key observation driving our approach is the ubiquity of VAEs in the architecture of LDMs. VAEs serve as a foundational component across different LDM implementations, often with only minor variations between models. For instance, the VAE used in Stable Diffusion 2.0 is essentially a fine-tuned version of the one employed in Stable Diffusion 1.5. This commonality presents a strategic opportunity: by focusing on the VAE, we can potentially affect a wide range of LDMs without requiring detailed knowledge of their specific architectures.

VAE can be considered as a probabilistic generative extension of the ordinary autoencoders. The encoder of a VAE aims at approximating the intractable posterior distribution of the latent variable  $\mathbf{z}$  by a Gaussian distribution  $q(\mathbf{z}|\mathbf{x}) = \mathcal{N}(\boldsymbol{\mu}, \text{diag}(\boldsymbol{\sigma}^2))$ , where  $\text{diag}$  denotes a diagonal

matrix formed with vector  $\sigma^2$  as the diagonal entries. The training proceeds by minimising the KL divergence between the approximating variational distribution  $q(\mathbf{z})$  and the true posterior  $p(\mathbf{z}|\mathbf{x})$ , and the learning objective is:

$$\mathcal{L}(\mathbf{x}) = -\mathbb{E}_{q(\mathbf{z}|\mathbf{x})} [\log p(\mathbf{x}, \mathbf{z}) - \ln q(\mathbf{z}|\mathbf{x})]. \quad (4)$$

The above loss is also known as negative ELBO. By observing the generating process  $p(\mathbf{x}, \mathbf{z}) = p(\mathbf{z})p(\mathbf{x}|\mathbf{z})$ , the loss can be written alternatively as:

$$\mathcal{L}(\mathbf{x}) = -\mathbb{E}_{q(\mathbf{z}|\mathbf{x})} [\ln p(\mathbf{x}|\mathbf{z})] + D_{\text{KL}}(q(\mathbf{z}|\mathbf{x}) \parallel p(\mathbf{z})), \quad (5)$$

where the first term is known as reconstruction error and the second term, the KL divergence between the variational distribution and the prior distribution, usually a standard normal distribution, that is  $p(\mathbf{z}) = \mathcal{N}(\mathbf{0}, \mathbf{I})$ . The KL divergence has a regularisation effect such that the variational distribution is ‘‘close’’ to a standard spherical Gaussian distribution.

By general consensus, training of VAE usually suffers an optimization issue called posterior collapsing (Razavi et al. 2019), that is the KL divergence term of Equation 5 dominates the overall loss such that all posteriors collapse to the uninformative prior and the reconstruction error or the likelihood term is ignored. We draw inspiration from this vulnerability and aim to propose adversarial attacks to cause the posterior collapse during inference stage.

**Posterior Collapse Loss Function.** We aim to leverage the divergence measure between  $q(\mathbf{z}|\mathbf{x})$  and a target distribution  $p^*(\mathbf{z})$ . The objective is to generate  $\mathbf{x}_{adv}$  by minimizing the KL divergence between  $q(\mathbf{z}|\mathbf{x})$  and  $p^*(\mathbf{z})$ . The KL divergence of two multivariate Gaussian distributions is:

$$D_{\text{KL}}(\mathcal{N}_1 \parallel \mathcal{N}_2) = \frac{1}{2} [\ln \frac{|\Sigma_2|}{|\Sigma_1|} - d + \text{tr}\{\Sigma_2^{-1}\Sigma_1\} + (\boldsymbol{\mu}_2 - \boldsymbol{\mu}_1)^T \Sigma_2^{-1} (\boldsymbol{\mu}_2 - \boldsymbol{\mu}_1)], \quad (6)$$

where  $\mathcal{N}_1 = \mathcal{N}(\boldsymbol{\mu}_1, \Sigma_1)$ ,  $\mathcal{N}_2 = \mathcal{N}(\boldsymbol{\mu}_2, \Sigma_2)$ .

For this work, we set the attack target  $p^*(\mathbf{z})$  to a zero mean Gaussian distribution  $p(\mathbf{z}) = \mathcal{N}(\mathbf{0}, v\mathbf{I})$ , where  $v > 0$  is hyper-parameter that controls the disruptive effect. Since both  $p^*(\mathbf{z})$  and  $q(\mathbf{z}|\mathbf{x})$  are diagonal multivariate Gaussian distributions, Equation 6 becomes:

$$\begin{aligned} \mathcal{L}_{\text{KL}}(\mathbf{x}) &= D_{\text{KL}}(q(\mathbf{z}|\mathbf{x}) \parallel p^*(\mathbf{z})) \\ &= \frac{1}{2} \sum_{i=1}^d \left( \frac{\sigma_i^2 + \mu_i^2}{v} - 1 + \ln \left( \frac{v}{\sigma_i^2} \right) \right). \end{aligned} \quad (7)$$

Therefore, the attack formulation becomes:

$$\min_{\boldsymbol{\delta}} \mathcal{L}_{\text{KL}}(\mathbf{x} + \boldsymbol{\delta}) \quad \text{s.t.} \quad \|\boldsymbol{\delta}\|_{\infty} < \epsilon. \quad (8)$$

Note that the attack target distribution is independent from the input image  $\mathbf{x}$ , making it a more general attack method. Successful attacks should make the encoded posterior uninformative or collapsed for a perturbed image, consequentially, the downstream image generation, i.e. Objective 2, will be disrupted accordingly as well.

Note that we choose to introduce the loss  $\mathcal{J}$  with  $f$ -divergence for its generality. Both forward KL and reverse

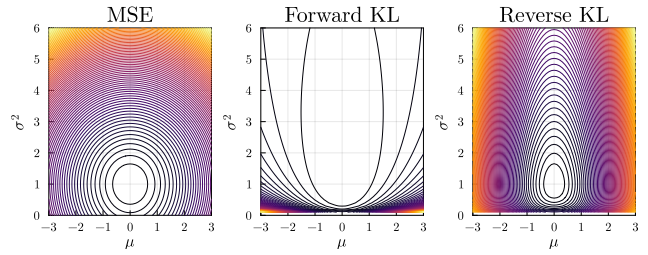


Figure 3: Comparison of impact on the gradient regarding different criterion.

KL are specific cases of the general divergence measure. For example, the reverse KL divergence is recovered when we set  $f = \ln$ . Comparing with the forward KL, the reverse KL, which is used in defining the VAE training loss and therefore also contributes to the posterior collapse issue, is found to perform better in disrupting the image generation. To see why, the reverse KL’s expectation is taken w.r.t  $q(\mathbf{z}|\mathbf{x}) = \mathcal{N}(\boldsymbol{\mu}, \text{diag}(\sigma^2))$ , making the attack objective more dependent on the encoding mean and variance rather than the fixed hyperparameter  $v$ . Three different loss measures, mean squared error, forward KL and reverse KL, are plotted in Figure 3, where the attack variance hyperparameter  $v$  is set to unit for convenience. As expected, all three losses have the same minimum:  $\mu = 0, \sigma^2 = 1$ . However, it can be observed that the reverse KL provides a more nuanced loss compared with the symmetric MSE error. In comparison with the forward loss, reverse KL’s loss surface provides more geometric information to guide the attack, which is manifested in the steeper gradient directions across the input domain. Thus, adversary generation can be achieved by maximizing the distributional gap using gradient ascent.

To craft adversarial samples, we use projected sign gradient ascent (Madry et al. 2018) for iterative updates. Our approach is inspired by the counterintuitive finding from Xue et al. (2024), where minimizing their loss function, contrary to the intuitive maximization, yielded better results. Following this insight, we explore both gradient directions by altering the sign of our final loss function, which will be discussed in appendix. Our update process follows the form:

$$\mathbf{x}^{t+1} = \mathcal{P}_{\ell_{\infty}^{\epsilon}(\boldsymbol{\delta}^t)}^{\epsilon} \left( \mathbf{x}^t + \alpha \text{sign} \nabla_{\mathbf{x}^t} \mathcal{J}(\mathbf{x}^t) \right), \quad (9)$$

where  $\mathcal{P}_{\ell_{\infty}^{\epsilon}(\boldsymbol{\delta}^t)}^{\epsilon}(\cdot)$  will apply the projection on  $\boldsymbol{\delta}^t$  in the  $\epsilon$ -ball of  $\ell_{\infty}$  norm,  $\alpha$  is a hyperparameter to adjust the learning rate during the optimization.

## Results

### Experiments Setup

**Dataset.** In our experiments, we utilized a 1000-image-subset of the ImageNet (Deng et al. 2009), as selected by Lin et al. (2020a). This choice aligns with established conventions in adversarial attack research. All images were resized to  $512 \times 512$ , ensuring consistency across evaluations.

**Baselines.** We compared our approach against several state-of-the-art methods, AdvDM (Liang et al. 2023), PhotoGuard (PG) (Salman et al. 2023), MIST (Liang and Wu

prompt	method	PSNR $\uparrow$		FID $\downarrow$		SSIM $\uparrow$		LPIPS $\downarrow$		ACDM $\downarrow$	
		SD14	SD15	SD14	SD15	SD14	SD15	SD14	SD15	SD14	SD15
P1	AdvDM	20.49	20.49	<u>153.71</u>	<u>150.22</u>	<b>0.4422</b>	<b>0.4417</b>	0.5010	0.5008	0.0416	0.0424
	PG	<u>18.49</u>	<u>18.52</u>	151.75	147.85	0.4800	0.4840	0.5647	<u>0.5629</u>	0.0786	0.0792
	MIST	18.50	18.54	150.20	147.78	0.4759	0.4797	0.5604	<u>0.5585</u>	0.0751	0.0757
	SDS	20.60	20.56	<b>155.55</b>	<b>152.76</b>	0.4519	0.4495	0.4998	0.5007	0.0453	0.0462
	Ours	<b>18.02</b>	<b>18.02</b>	139.11	135.32	<u>0.4441</u>	<u>0.4453</u>	<b>0.6188</b>	<b>0.6171</b>	<b>0.1106</b>	<b>0.1110</b>
P2	AdvDM	19.23	19.25	<u>94.90</u>	<u>92.09</u>	<b>0.4226</b>	<b>0.4232</b>	0.5017	0.5001	0.0442	0.0440
	PG	<u>17.32</u>	<u>17.31</u>	88.43	91.00	0.4650	0.4660	<u>0.5585</u>	<u>0.5592</u>	<u>0.0858</u>	<u>0.0865</u>
	MIST	<u>17.32</u>	17.32	88.17	88.87	0.4616	0.4632	0.5539	<u>0.5552</u>	0.0830	0.0837
	SDS	19.32	19.31	<b>99.80</b>	<b>99.03</b>	<u>0.4312</u>	<u>0.4304</u>	0.5035	0.5029	0.0480	0.0483
	Ours	<b>16.74</b>	<b>16.70</b>	70.59	69.04	0.4336	0.4329	<b>0.6005</b>	<b>0.5990</b>	<b>0.1156</b>	<b>0.1167</b>
P3	AdvDM	19.37	19.42	143.57	140.01	<u>0.4291</u>	<u>0.4298</u>	0.5142	0.5102	0.0454	0.0452
	PG	<u>17.26</u>	<u>17.22</u>	123.94	127.87	0.4702	0.4749	<u>0.5727</u>	<u>0.5727</u>	<u>0.0847</u>	<u>0.0853</u>
	MIST	17.27	17.18	121.36	127.34	0.4685	0.4732	0.5691	0.5687	0.0820	0.0829
	SDS	19.56	19.59	<u>144.63</u>	<u>144.64</u>	0.4409	0.4385	0.5128	0.5102	0.0492	0.0491
	Ours	<b>16.71</b>	<b>16.78</b>	<b>156.47</b>	<b>153.85</b>	<b>0.4234</b>	<b>0.4228</b>	<b>0.6202</b>	<b>0.6204</b>	<b>0.1084</b>	<b>0.1079</b>
P4	AdvDM	19.32	19.31	148.26	145.27	<u>0.4045</u>	<u>0.4040</u>	0.5347	0.5324	0.0488	0.0486
	PG	<u>17.87</u>	<u>17.84</u>	<b>150.85</b>	<b>151.75</b>	0.4560	0.4589	<u>0.5820</u>	<u>0.5818</u>	<u>0.0804</u>	<u>0.0819</u>
	MIST	17.88	17.85	148.64	<u>150.45</u>	0.4526	0.4540	0.5786	0.5788	0.0770	0.0786
	SDS	19.49	19.48	<u>149.37</u>	148.82	0.4196	0.4176	0.5293	0.5275	0.0522	0.0520
	Ours	<b>17.61</b>	<b>17.50</b>	116.48	115.41	<b>0.4004</b>	<b>0.3942</b>	<b>0.6361</b>	<b>0.6394</b>	<b>0.1051</b>	<b>0.1067</b>
P5	AdvDM	19.41	19.33	<u>159.45</u>	<u>166.76</u>	<b>0.4088</b>	<b>0.4076</b>	0.5239	0.5226	0.0445	0.0441
	PG	<u>17.77</u>	<u>17.80</u>	110.96	112.49	0.5091	0.4988	<u>0.5460</u>	<u>0.5517</u>	<u>0.0945</u>	<u>0.0924</u>
	MIST	17.81	17.82	107.88	110.79	0.5087	0.4972	0.5404	0.5459	0.0915	0.0892
	SDS	19.48	19.39	<b>162.63</b>	<b>170.77</b>	<u>0.4171</u>	<u>0.4149</u>	0.5239	0.5236	0.0487	0.0485
	Ours	<b>16.81</b>	<b>16.95</b>	134.71	129.93	0.4568	0.4524	<b>0.6032</b>	<b>0.6047</b>	<b>0.1227</b>	<b>0.1209</b>

Table 1: Comparison of our method against several baselines. Arrows ( $\uparrow/\downarrow$ ) indicate whether higher or lower values represent better image quality for each image quality metric. Data is grouped vertically in sets of four for each metric and model. The **best result** in each group is in bold, and the second-best result is underlined.

2023), and SDS (Xue et al. 2024). To ensure a fair comparison, we use the gradient ascent version of SDS, aligning with the optimization settings of other methods. We fix  $t = 40$  and  $\epsilon = 16$  for all methods, the rest left default. We implement our method with  $\alpha = 2$ ,  $v = 1 \times 10^{-8}$ , the optimization follows the goal defined in Equation 8, which the opposite one will be illustrated in Appendix.

**Victim Models.** Our experiments primarily focused on popular LDMs, specifically the lightweight Stable Diffusion 1.4 (SD14) and 1.5 (SD15). These models were chosen due to their widespread accessibility and higher potential for misuse, making them relevant targets for our study on protecting against unauthorized image manipulation. To assess the transferability across different resolution and architectures, we also tested the first 100 images on Stable Diffusion 2.0 (SD20) with  $768 \times 768$ , and Stable Diffusion XL (SDXL) with  $1024 \times 1024$  for all methods. All reported results of our method leverage the VAE of SD15 as the surrogate model.

**Varied Prompts.** To further evaluate the robustness and versatility of our method, we conducted inference using a diverse set of prompts. These prompts include: **P1**: an empty prompt; **P2**: a caption generated by BLIP (Li et al. 2022) with the clean image; **P3**: “*add some snow*” to represent weather modifications; **P4**: “*apply sunset lighting*” to test lighting adjustments; **P5**: “*make it like a watercolor paint-*

*ing*” to examine style transfer capabilities. Through this varied set of prompts, we aimed to assess our method’s effectiveness across a wide range of potential image manipulation scenarios.

**Image Quality Assessment (IQA).** To quantitatively assess the quality of the edited images pre- and post-attack, we employed five different IQAs. Peak Signal-to-Noise Ratio (PSNR) provides insight into the overall distortion introduced. Fréchet Inception Distance (FID) offers a measure of the perceptual quality and generation diversity (Heusel et al. 2017). Structural Similarity Index (SSIM) captures changes in local patterns of pixel intensities (Wang et al. 2004). Learned Perceptual Image Patch Similarity (LPIPS) approximately measures human perceptual similarities (Zhang et al. 2018). Aesthetic Color Distance Metric (ACDM) evaluates the overall color consistency (Guo et al. 2024b).

**Against Defending Methods.** To evaluate our attack’s robustness against potential defenses, we considered two methods. First, we examined Adv-Clean<sup>1</sup>, a filter-based approach designed to remove adversarial perturbations in diffusion models without requiring additional training. Second, we applied  $3 \times 3$  Gaussian blur to simulate potential degradation of protected images during the distribution. We apply

<sup>1</sup><https://huggingface.co/spaces/platdev/AdverseCleaner>

these defense on our attacked images and evaluate on SD15.

### Image Editing Results with Varied Prompts

Our experimental results demonstrate the superior performance of our proposed PCA compared to existing methods. Figure 2 provides a visual comparison, while Table 1 presents quantitative results.

As observed from Figure 2, our method significantly outperforms existing approaches in terms of semantic disruption. Most other methods largely maintain an image structure similar to that of the clean image after editing. In contrast, our approach fundamentally alters the semantic information of the image, resulting in edited outputs that bear almost no resemblance to the infringer-desired images.

Even when prompts containing image structure information are provided, our method continues to demonstrate superior performance. The generated images show significant discrepancies from the expected outcomes, effectively thwarting attempts at unauthorized manipulation. Moreover, our approach introduces quite noise patterns in the generated images, substantially degrading their quality. This degradation renders the manipulated images unsuitable for their intended purposes, whether it be unauthorized use, redistribution, or further editing. Our method not only disrupts the semantic content of the image but also compromises its overall visual quality. This comprehensive degradation ensures that even if an attacker manages to partially reconstruct some elements of the original image, the result remains unusable from both a semantic and aesthetic standpoint.

The quantitative results in Table 1 further corroborate the effectiveness of our method. Notably, our Posterior Collapse Attack achieves state-of-the-art results while requiring minimal knowledge of the opponent model, less computational time, and lower GPU memory usage compared to existing methods (as illustrated in Figure 1).

These results demonstrate that, our approach effectively disrupts image semantics while maintaining efficiency and generalizability. This strategy challenges generative models’ ability to produce coherent edits, operating with minimal model-specific information in a near black-box scenario.

### Transferability

As shown in Figure 4, our method demonstrates superior transferability compared to existing approaches when tested on both SD20 and SDXL models. Across all five IQA metrics, our approach consistently achieves the highest normalized scores of 1.0, indicating the best attack performance. In contrast, other methods show varying degrees of effectiveness, with PhotoGuard and MIST performing moderately well, while AdvDM and SDS exhibit limited transferability. These results validate our hypothesis regarding the limitations of current protection techniques that rely heavily on white-box access to target models. Our method, by minimizing dependence on model-specific knowledge, achieves better performance across diverse model architectures. This generalizability is crucial in addressing the challenges posed by rapidly evolving generative AI models, offering a more practical and enduring solution in this dynamic field.

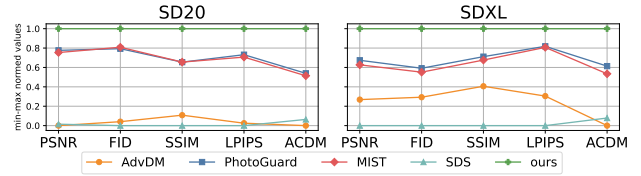


Figure 4: Transferability results of 5 methods on SD20 and SDXL. Results are averaged across five prompts per method. All IQA metrics are min-max normalized or 1 – min-max normalized, with higher values consistently indicating better attack performance.

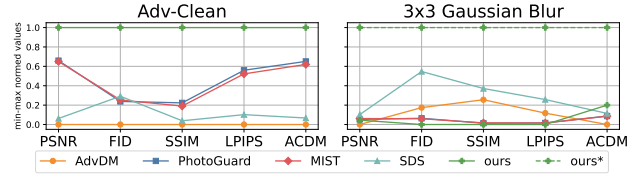


Figure 5: Attack performance after Adv-Clean and JPEG degrade defense, where \* indicates the adaptive version of the method. The data in this figure under the same normalization as Figure 4 for better visualization.

### Against Defense

As shown in Figure 5, our method demonstrates robust performance against the Adv-Clean defense, consistently achieving the highest normalized scores of 1.0 across all five IQA metrics. This indicates superior resilience to this type of defense compared to other methods. PhotoGuard and MIST show moderate effectiveness, while AdvDM and SDS exhibit limited resistance to Adv-Clean. Against  $3 \times 3$  Gaussian blur, our original method shows comparable performance, particularly in PSNR and ACDM, indicating resilience in overall image quality and color manipulation. With a simple adaptive attack technique (denoted as ours\*), our method achieves superior performance across all metrics, consistently outperforming other approaches. This improvement demonstrates our approach’s flexibility and robustness. While the non-adaptive version has already performed well in some metrics, the adaptive version’s dominance across all metrics highlights our method’s ability to maintain effectiveness under various defenses. This adaptation allowing our method to quickly recover its original performance when under specific defense strategy. These results underscore the versatility of our attack strategy, proving its capability to overcome diverse defense mechanisms with or without minor adjustments.

### Conclusion

In this paper, we proposed the Posterior Collapse Attack, a novel method for disrupting LDM-based image editing, requiring fewer parameters — merely 3.39% of the whole model, which makes our method operate faster and consumes less VRAM than existing approaches. We leverage a

novel loss function targeting the VAE encoder of LDMs, induces collapse in the VAE’s posterior distribution to significant disrupt the image semantic during LDM editing. Experimental results demonstrate that PCA significantly degrades the quality of LDM-edited images, causing a collapse in their semantic content. This approach proves highly effective in protecting images from unauthorized manipulation across various LDM architectures. Our work contributes to the ongoing efforts to secure digital assets in an era of rapidly advancing generative AI, alleviating the socio-technical challenges posed by malicious AI misuse.

## References

- Deng, J.; Dong, W.; Socher, R.; Li, L.-J.; Li, K.; and Fei-Fei, L. 2009. Imagenet: A large-scale hierarchical image database. In *2009 IEEE conference on computer vision and pattern recognition (CVPR)*, 248–255. Ieee.
- Dhariwal, P.; and Nichol, A. 2021. Diffusion models beat gans on image synthesis. *Advances in Neural Information Processing Systems*, 34: 8780–8794.
- Dosovitskiy, A.; and Brox, T. 2016. Generating images with perceptual similarity metrics based on deep networks. *Advances in Neural Information Processing Systems*, 29.
- Esser, P.; Rombach, R.; and Ommer, B. 2021. Taming Transformers for High-Resolution Image Synthesis. In *Proceedings of the IEEE/CVF Conference on Computer Vision and Pattern Recognition (CVPR)*, 12873–12883.
- Gondim-Ribeiro, G.; Tabacof, P.; and Valle, E. 2018. Adversarial attacks on variational autoencoders. *arXiv preprint arXiv:1806.04646*.
- Goodfellow, I. J.; Shlens, J.; and Szegedy, C. 2015. Explaining and Harnessing Adversarial Examples. In *International Conference on Learning Representations*.
- Guo, Z.; Li, W.; Qian, Y.; Arandjelovic, O.; and Fang, L. 2024a. A White-Box False Positive Adversarial Attack Method on Contrastive Loss Based Offline Handwritten Signature Verification Models. In *International Conference on Artificial Intelligence and Statistics*, 901–909. PMLR.
- Guo, Z.; Wang, K.; Li, W.; Qian, Y.; Arandjelović, O.; and Fang, L. 2024b. Artwork protection against neural style transfer using locally adaptive adversarial color attack. *arXiv preprint arXiv:2401.09673*.
- Heusel, M.; Ramsauer, H.; Unterthiner, T.; Nessler, B.; and Hochreiter, S. 2017. Gans trained by a two time-scale update rule converge to a local nash equilibrium. *Advances in Neural Information Processing Systems*, 30.
- Ho, J.; Jain, A.; and Abbeel, P. 2020. Denoising diffusion probabilistic models. *Advances in Neural Information Processing Systems*, 33: 6840–6851.
- Isola, P.; Zhu, J.-Y.; Zhou, T.; and Efros, A. A. 2017. Image-To-Image Translation With Conditional Adversarial Networks. In *Proceedings of the IEEE Conference on Computer Vision and Pattern Recognition (CVPR)*.
- Kingma, D.; Salimans, T.; Poole, B.; and Ho, J. 2021. Variational diffusion models. *Advances in Neural Information Processing Systems*, 34: 21696–21707.
- Kos, J.; Fischer, I.; and Song, D. 2018. Adversarial examples for generative models. In *2018 IEEE Security and Privacy Workshops (SPW)*, 36–42. IEEE.
- Kuzina, A.; Welling, M.; and Tomczak, J. 2022. Alleviating adversarial attacks on variational autoencoders with mcmc. *Advances in Neural Information Processing Systems*, 35: 8811–8823.
- Lau, C. P.; Liu, J.; Lin, W.-A.; Souri, H.; Khorramshahi, P.; and Chellappa, R. 2023a. Adversarial attacks and robust defenses in deep learning. In *Handbook of Statistics*, volume 48, 29–58. Elsevier.
- Lau, C. P.; Liu, J.; Souri, H.; Lin, W.-A.; Feizi, S.; and Chellappa, R. 2023b. Interpolated joint space adversarial training for robust and generalizable defenses. *IEEE Transactions on Pattern Analysis and Machine Intelligence*, 45(11): 13054–13067.
- Li, J.; Li, D.; Xiong, C.; and Hoi, S. 2022. Blip: Bootstrapping language-image pre-training for unified vision-language understanding and generation. In *International Conference on Machine Learning*, 12888–12900. PMLR.
- Li, Y.; Hu, J.; Guo, Z.; Yang, N.; Chen, H.; Yuan, D.; and Ding, W. 2024. Threats and Defenses in Federated Learning Life Cycle: A Comprehensive Survey and Challenges. *arXiv preprint arXiv:2407.06754*.
- Liang, C.; and Wu, X. 2023. Mist: Towards improved adversarial examples for diffusion models. *arXiv preprint arXiv:2305.12683*.
- Liang, C.; Wu, X.; Hua, Y.; Zhang, J.; Xue, Y.; Song, T.; Xue, Z.; Ma, R.; and Guan, H. 2023. Adversarial Example Does Good: Preventing Painting Imitation from Diffusion Models via Adversarial Examples. In *International Conference on Machine Learning*, 20763–20786. PMLR.
- Lin, J.; Song, C.; He, K.; Wang, L.; and Hopcroft, J. E. 2020a. Nesterov Accelerated Gradient and Scale Invariance for Adversarial Attacks. In *International Conference on Learning Representations*.
- Lin, W.-A.; Lau, C. P.; Levine, A.; Chellappa, R.; and Feizi, S. 2020b. Dual manifold adversarial robustness: Defense against lp and non-lp adversarial attacks. *Advances in Neural Information Processing Systems*, 33: 3487–3498.
- Liu, J.; Wei, C.; Guo, Y.; Yu, H.; Yuille, A.; Feizi, S.; Lau, C. P.; and Chellappa, R. 2023. Instruct2Attack: Language-Guided Semantic Adversarial Attacks. *arXiv preprint arXiv:2311.15551*.
- Madry, A.; Makelov, A.; Schmidt, L.; Tsipras, D.; and Vladu, A. 2018. Towards Deep Learning Models Resistant to Adversarial Attacks. In *International Conference on Learning Representations*.
- Paszke, A.; Gross, S.; Massa, F.; Lerer, A.; Bradbury, J.; Chanan, G.; Killeen, T.; Lin, Z.; Gimelshein, N.; Antiga, L.; et al. 2019. Pytorch: An imperative style, high-performance deep learning library. *Advances in Neural Information Processing Systems*, 32.
- Picard, D. 2021. Torch. manual\_seed (3407) is all you need: On the influence of random seeds in deep learning architectures for computer vision. *arXiv preprint arXiv:2109.08203*.



- Razavi, A.; van den Oord, A.; Poole, B.; and Vinyals, O. 2019. Preventing Posterior Collapse with delta-VAEs. In *International Conference on Learning Representations*.
- Razavi, A.; Van den Oord, A.; and Vinyals, O. 2019. Generating diverse high-fidelity images with vq-vae-2. *Advances in Neural Information Processing Systems*, 32.
- Rombach, R.; Blattmann, A.; Lorenz, D.; Esser, P.; and Ommer, B. 2022. High-Resolution Image Synthesis With Latent Diffusion Models. In *Proceedings of the IEEE/CVF Conference on Computer Vision and Pattern Recognition (CVPR)*, 10684–10695.
- Salman, H.; Khaddaj, A.; Leclerc, G.; Ilyas, A.; and Madry, A. 2023. Raising the cost of malicious AI-powered image editing. In *Proceedings of the 40th International Conference on Machine Learning*, 29894–29918.
- Shan, S.; Cryan, J.; Wenger, E.; Zheng, H.; Hanoeka, R.; and Zhao, B. Y. 2023. Glaze: Protecting artists from style mimicry by {Text-to-Image} models. In *32nd USENIX Security Symposium (USENIX Security 23)*, 2187–2204.
- Simonyan, K.; and Zisserman, A. 2015. Very Deep Convolutional Networks for Large-Scale Image Recognition. In *International Conference on Learning Representations*.
- Song, J.; Meng, C.; and Ermon, S. 2021. Denoising Diffusion Implicit Models. In *International Conference on Learning Representations*.
- Sezgedy, C.; Zaremba, W.; Sutskever, I.; Bruna, J.; Erhan, D.; Goodfellow, I.; and Fergus, R. 2014. Intriguing Properties of Neural Networks. In *International Conference on Learning Representations*.
- Tabacof, P.; Tavares, J.; and Valle, E. 2016. Adversarial images for variational autoencoders. *arXiv preprint arXiv:1612.00155*.
- von Platen, P.; Patil, S.; Lozhkov, A.; Cuenca, P.; Lambert, N.; Rasul, K.; Davaadorj, M.; Nair, D.; Paul, S.; Berman, W.; Xu, Y.; Liu, S.; and Wolf, T. 2022. Diffusers: State-of-the-art diffusion models. <https://github.com/huggingface/diffusers>.
- Wang, Z.; Bovik, A. C.; Sheikh, H. R.; and Simoncelli, E. P. 2004. Image quality assessment: from error visibility to structural similarity. *IEEE Transactions on Image Processing*, 13(4): 600–612.
- Xue, H.; Liang, C.; Wu, X.; and Chen, Y. 2024. Toward effective protection against diffusion-based mimicry through score distillation. In *The Twelfth International Conference on Learning Representations*.
- Yan, W.; Zhang, Y.; Abbeel, P.; and Srinivas, A. 2021. Videogpt: Video generation using vq-vae and transformers. *arXiv preprint arXiv:2104.10157*.
- Yu, J.; Li, X.; Koh, J. Y.; Zhang, H.; Pang, R.; Qin, J.; Ku, A.; Xu, Y.; Baldridge, J.; and Wu, Y. 2022. Vector-quantized Image Modeling with Improved VQGAN. In *International Conference on Learning Representations*.
- Zhang, R.; Isola, P.; Efros, A. A.; Shechtman, E.; and Wang, O. 2018. The Unreasonable Effectiveness of Deep Features as a Perceptual Metric. In *Proceedings of the IEEE Conference on Computer Vision and Pattern Recognition (CVPR)*.
- Zhao, S.; Jia, M.; Guo, Z.; Gan, L.; Fu, J.; Feng, Y.; Pan, F.; and Tuan, L. A. 2024. A Survey of Backdoor Attacks and Defenses on Large Language Models: Implications for Security Measures. *arXiv preprint arXiv:2406.06852*.

# Appendix

## Derivation of the Loss Function

For the Equation 6 to Equation 7 in the main paper, we provide a derivation to demonstrate how we obtained Equation 7 from Equation 6:

Given two multivariate Gaussian distribution  $\mathcal{N}_1(\boldsymbol{\mu}_1, \boldsymbol{\Sigma}_1)$  and  $\mathcal{N}_2(\boldsymbol{\mu}_2, \boldsymbol{\Sigma}_2)$ , where  $\mathcal{N}_1$  and  $\mathcal{N}_2$  refer to the posterior distribution  $q(\mathbf{z}|\mathbf{x})$  and our target prior distribution  $p^*(\mathbf{z})$ . We set the target attack  $p^*(\mathbf{z})$  to a zero mean Gaussian distribution  $p^*(\mathbf{z}) = \mathcal{N}(\mathbf{0}, v\mathbf{I})$ . Since both  $p^*(\mathbf{z})$  and  $q(\mathbf{z}|\mathbf{x})$  are diagonal multivariate Gaussian distributions, equation can be derived as:

$$\begin{aligned} D_{\text{KL}}(\mathcal{N}_1 \parallel \mathcal{N}_2) &= \frac{1}{2} \left[ \ln \frac{|\boldsymbol{\Sigma}_2|}{|\boldsymbol{\Sigma}_1|} - d + \text{tr} \{ \boldsymbol{\Sigma}_2^{-1} \boldsymbol{\Sigma}_1 \} + (\boldsymbol{\mu}_2 - \boldsymbol{\mu}_1)^T \boldsymbol{\Sigma}_2^{-1} (\boldsymbol{\mu}_2 - \boldsymbol{\mu}_1) \right] \\ &= \frac{1}{2} \left( \ln \prod_{i=1}^d \frac{v}{\sigma_i^2} - d + \sum_{i=1}^d \frac{\sigma_i^2}{v} + \frac{\boldsymbol{\mu}^T \boldsymbol{\mu}}{v} \right) \\ &= \frac{1}{2} \left( \sum_{i=1}^d \ln \frac{v}{\sigma_i^2} - d + \sum_{i=1}^d \frac{\sigma_i^2}{v} + \sum_{i=1}^d \frac{\mu_i^2}{v} \right) \\ &= \frac{1}{2} \sum_{i=1}^d \left( \ln \frac{v}{\sigma_i^2} - 1 + \frac{\mu_i^2 + \sigma_i^2}{v} \right). \end{aligned}$$

Notably, in our implementation, we ignore the  $\ln v$  term, because  $\ln v$  is a constant, which will not influence the performance. Therefore, the final loss function in our implementation is:

$$D_{\text{KL}}(\mathcal{N}_1 \parallel \mathcal{N}_2) \simeq \mathcal{L}_{\text{KL}}(\mathbf{x}) = \frac{1}{2} \sum_{i=1}^d \left( -\ln \sigma_i^2 - 1 + \frac{\mu_i^2 + \sigma_i^2}{v} \right).$$

## Gradient Direction

As briefly mentioned in the main paper, our investigation was motivated by the work of Xue et al. (2024), leading us to examine both the minimization (-) and maximization (+) of the loss function  $\mathcal{L}_{\text{KL}}$ .

To provide context for our analysis, we revisit the two primary objectives outlined in the main paper:

**Objective 1:**  $\min_{\boldsymbol{\delta}} \mathcal{D}(f(\mathbf{x} + \boldsymbol{\delta}), \mathbf{x} + \mathbf{w})$  s.t.  $\|\boldsymbol{\delta}\|_p \leq \epsilon$ ,

**Objective 2:**  $\max_{\boldsymbol{\delta}} \mathcal{D}(f(\mathbf{x} + \boldsymbol{\delta}), f(\mathbf{x}))$  s.t.  $\|\boldsymbol{\delta}\|_p \leq \epsilon$ .

It is crucial to note that these objectives, while seemingly different, share a common goal: to prevent the infringer-desired output. This commonality allows us to consider Objective 1 as a variant of Objective 2.

For a comprehensive evaluation of our method’s performance, we employ two distinct approaches:

- **Evaluation of Objective 1:**

We compute IQAs between clean images and edited adversarial samples, represented as  $\text{IQA}(\mathbf{x}, f(\mathbf{x}_{adv}))$ . This approach aligns with some baselines studies (Liang et al. 2023; Xue et al. 2024).

- **Evaluation of Objective 2:**

We calculate IQAs between edited clean images and edited adversarial samples, denoted as  $\text{IQA}(f(\mathbf{x}), f(\mathbf{x}_{adv}))$ . This metric is consistent with the results presented in the main paper.

## Two Variants of Posterior Collapse

Posterior collapse in VAEs is a phenomenon that can manifest in two primary forms: diffusion collapse and concentration collapse. Let  $\mathcal{X}$  be the input space and  $\mathcal{Z} \subseteq \mathbb{R}^d$  be the latent space of a VAE. The posterior distribution in a VAE is denoted by  $q(\mathbf{z} | \mathbf{x})$ , where  $\mathbf{x} \in \mathcal{X}$  and  $\mathbf{z} \in \mathcal{Z}$ .

Here we give definitions of two kind of collapses and explain when the phenomena will occur:

1. **Diffusion Collapse:**

We witness diffusion collapse when the posterior distribution becomes overly dispersed:

$$q(\mathbf{z} | \mathbf{x}) \approx \mathcal{U}(\mathcal{Z}) \quad \text{as} \quad \sigma^2 \rightarrow \infty, \tag{10}$$

where  $\mathcal{U}(\mathcal{Z})$  denotes the uniform distribution over  $\mathcal{Z}$ . In this case, the encoder produces highly uncertain latent representations for all inputs.

## 2. Concentration Collapse:

In this scenario, the posterior distribution becomes excessively concentrated, approaching a Dirac delta function:

$$q(\mathbf{z} | \mathbf{x}) \rightarrow \delta(\mathbf{z} - \boldsymbol{\mu}_0) \quad \text{as} \quad \boldsymbol{\mu}, \boldsymbol{\sigma}^2 \rightarrow \mathbf{0}, \quad (11)$$

where  $\delta$  is the Dirac delta function, and  $\boldsymbol{\mu}_0$  is typically the mean of the prior distribution. This collapse results in the encoder mapping all inputs to nearly identical latent representations.

Based on the above definitions, we propose two strategies to cause these two collapse phenomena:

### 1. Maximization Strategy (PCA+):

Consider the optimization problem:

$$\max_{\boldsymbol{\delta}} \mathcal{L}_{\text{KL}}(\mathbf{x} + \boldsymbol{\delta}) \quad \text{s.t.} \quad \|\boldsymbol{\delta}\|_{\infty} < \epsilon. \quad (12)$$

When  $v = 1$ , the KL divergence simplifies to:

$$\mathcal{L}_{\text{KL}}(\mathbf{x}) = \frac{1}{2} \sum_{i=1}^d (-\ln \sigma_i^2 - 1 + \mu_i^2 + \sigma_i^2). \quad (13)$$

Analysis shows that maximizing this leads to:

$$|\mu_i| \rightarrow \infty \quad \text{and} \quad \sigma_i^2 \rightarrow \infty \quad \text{for all } i, \quad (14)$$

resulting in diffusion collapse.

PCA+ optimization pushes the latent distribution  $\mathcal{N}(\boldsymbol{\mu}, \boldsymbol{\sigma}^2)$  away from the prior distribution  $\mathcal{N}(\mathbf{0}, \mathbf{I})$ , effectively creating an out-of-distribution (OOD) scenario. This divergence introduces a significant domain shift for the downstream diffusion model, moving the data distribution into regions where the model’s knowledge is limited or inaccurate. Consequently, the diffusion model struggles to perform proper inference on the transformed data, as its fundamental assumptions about the data distribution are violated.

This scenario can be conceptualized as an expansion of the latent space, where data is forced to extend beyond the normal domain of the downstream diffusion model’s understanding. This manipulation can be seen as a method to “confuse” the diffusion model by presenting it with data that falls outside its expected input distribution. The effect is analogous to creating a domain shift in the context of VAEs, where the latent space is manipulated to fall outside the expected distribution that the decoder was trained on.

Intuitively the downstream LDM will pay attention to move those OOD points into the known distribution, causing results consistent with Objective 1 expectations.

### 2. Minimization Strategy (PCA-):

Consider the optimization problem:

$$\min_{\boldsymbol{\delta}} \mathcal{L}_{\text{KL}}(\mathbf{x} + \boldsymbol{\delta}) \quad \text{s.t.} \quad \|\boldsymbol{\delta}\|_{\infty} < \epsilon. \quad (15)$$

As  $v \rightarrow 0^+$ , the dominant term becomes:

$$\frac{\mu_i^2 + \sigma_i^2}{v}. \quad (16)$$

Minimizing this expression leads to:

$$\mu_i \rightarrow 0 \quad \text{and} \quad \sigma_i^2 \rightarrow 0 \quad \text{for all } i, \quad (17)$$

resulting in concentration collapse.

PCA- forces the posterior distribution to converge towards  $\mathcal{N}(\mathbf{0}, \mathbf{0})$ , effectively collapsing the distribution into a point mass at  $\mathbf{z} = \mathbf{0}$ , a Dirac delta function centered at the origin of the latent space. In this context, as the distribution collapses, all latent representations are concentrated at  $\mathbf{z} = \mathbf{0}$ , leading to a severe loss of dimensionality in the latent space. The normal distribution  $\mathcal{N}(\mathbf{0}, \mathbf{0})$  ceases to be a valid probability distribution for describing the data, instead becoming a degenerate case where the distribution has zero variance in all dimensions.

When this collapsed distribution is passed through a LDM, it results in a complete breakdown of semantic information in the edited images. The LDM, expecting a meaningful distribution in the latent space, fails to generate coherent outputs from this degenerate input.

This collapse represents a total loss of information about the original data variability, matching the Objective 2, which makes it impossible for the LDM to recover meaningful features or structures.

## Notations

Throughout this section, we use the following nomenclature:

- “PCA-” and “ours-”: Refer to minimize the  $\mathcal{L}_{\text{KL}}$  (consistent with Table 1 in the main paper) with  $v = 1 \times 10^{-8}$
- “PCA+” and “ours+”: Refer to maximize the  $\mathcal{L}_{\text{KL}}$  with  $v = 1$

In the subsequent tables (Table 2 and Table 3), we employ the following conventions:

- **Gray background**: Indicates methods not compared with others
- **Bold text**: Denotes the best results
- Underlined text: Highlights the second-best results

Our extensive experimentation is consistent with the hypothesis: PCA+ is good at Objective 1, while PCA- excels in addressing Objective 2. The following sections delve deeper into these findings.

### Analysis of PCA+ Performance (Objective 1)

Table 2 presents a comprehensive comparison of  $\text{IQA}(\mathbf{x}, f(\mathbf{x}_{adv}))$  across various methods, highlighting the efficacy of our PCA+ approach. The results demonstrate a consistent superior performance of our method across multiple Image Quality Assessment (IQA) metrics. Notably, PCA+ achieves the best scores in PSNR, FID, SSIM, and LPIPS across all evaluated scenarios, indicating a robust ability to maintain similarity between the edited adversarial image and the original image.

While the PCA+ method does not lead in ACDM scores, it remains highly competitive, consistently ranking among the top-tier performers. This comprehensive performance across various metrics underscores the method’s effectiveness in addressing Objective 1.

Visual analysis, as evidenced in Figures 6 and Figure 7, reveals that PCA+ produces results visually comparable to established methods such as SDS and AdvDM. A characteristic feature observed in the edited images is the appearance of watermark artifacts, which is consistent across these methods. However, PCA+ distinguishes itself through enhanced resistance to undesired edits. This superiority is not only reflected in the quantitative metrics but also apparent in qualitative analysis. A striking example is observed in the P3 scenario, where PCA+ successfully prevents the appearance of snow-like artifacts in  $f(\mathbf{x}_{adv})$ , a feat not achieved by other methods.

### Analysis of PCA- Performance (Objective 2)

Table 3 provides a detailed comparison of  $\text{IQA}(f(\mathbf{x}), f(\mathbf{x}_{adv}))$  across different methods, showcasing the effectiveness of our PCA- approach in addressing Objective 2. The results reveal that PCA- achieves the highest level of disruption to the infringer-desired output among all evaluated methods.

Visual analysis of the results, as illustrated in Figures 6 and Figure 7, demonstrates a striking contrast between PCA- and other methods. Alternative approaches tend to preserve some degree of structural and color information similar to  $f(\mathbf{x})$  in their  $f(\mathbf{x}_{adv})$ , however, PCA- stands out by completely obliterating the semantic information of the edited image.

A concrete example of this capability is evident in Figure 6. In this instance, where other methods produce images still recognizable as pineapples post-editing, our PCA- method generates severely distorted images. These distortions introduce semantically unrelated content, such as rubble, meaningless patterns, and even unrelated objects like trees. This level of semantic destruction effectively renders the edited image unusable for the original, potentially infringing purpose, while maintaining the integrity of the protection mechanism.

prompt	method	PSNR $\uparrow$		FID $\downarrow$		SSIM $\uparrow$		LPIPS $\downarrow$		ACDM $\downarrow$	
		SD14	SD15	SD14	SD15	SD14	SD15	SD14	SD15	SD14	SD15
P1	clean	19.09	19.09	54.95	54.25	0.5911	0.5914	0.3948	0.3943	0.0243	0.0242
	AdvDM	16.93	16.93	<u>172.10</u>	169.12	0.2748	0.2746	0.5783	0.5778	<b>0.0503</b>	<b>0.0508</b>
	PG	15.83	15.87	179.36	175.49	<u>0.3170</u>	<u>0.3208</u>	0.6335	0.6318	0.0890	0.0894
	MIST	15.77	15.81	178.92	176.25	<u>0.3086</u>	<u>0.3125</u>	0.6314	0.6297	0.0859	0.0862
	SDS	<u>17.15</u>	<u>17.12</u>	172.47	169.68	0.2944	0.2924	0.5687	0.5690	<u>0.0523</u>	<u>0.0530</u>
	Ours-	15.84	15.87	165.78	161.62	0.2994	0.3031	0.6868	0.6841	0.1164	0.1168
	Ours+	<b>18.85</b>	<b>18.82</b>	<b>109.01</b>	<b>108.57</b>	<b>0.4424</b>	<b>0.4396</b>	<b>0.5349</b>	<b>0.5345</b>	0.0593	0.0601
P2	clean	18.68	18.69	45.34	45.41	0.5829	0.5838	0.3993	0.3986	0.0253	0.0251
	AdvDM	16.67	16.65	103.37	101.18	0.2826	0.2822	0.5658	0.5649	<b>0.0530</b>	<b>0.0526</b>
	PG	15.54	15.53	98.02	101.82	<u>0.3438</u>	<u>0.3465</u>	0.6176	0.6176	0.0929	0.0933
	MIST	15.49	15.50	98.56	<u>99.92</u>	0.3359	0.3398	0.6154	0.6154	0.0902	0.0909
	SDS	<u>16.89</u>	<u>16.85</u>	107.53	106.82	0.3009	0.2993	<u>0.5587</u>	<u>0.5585</u>	<u>0.0555</u>	<u>0.0555</u>
	Ours-	15.32	15.30	81.17	80.16	0.3371	0.3347	0.6575	0.6564	0.1184	0.1197
	Ours+	<b>18.61</b>	<b>18.60</b>	<b>70.40</b>	<b>70.08</b>	<b>0.4460</b>	<b>0.4444</b>	<b>0.5276</b>	<b>0.5269</b>	0.0602	0.0608
P3	clean	18.50	18.54	78.89	78.98	0.5722	0.5735	0.4284	0.4281	0.0268	0.0266
	AdvDM	16.54	16.53	170.08	169.18	0.2734	0.2726	0.5852	0.5823	<b>0.0538</b>	<b>0.0536</b>
	PG	15.23	15.21	173.28	177.95	<u>0.3371</u>	<u>0.3414</u>	0.6342	0.6342	0.0938	0.0940
	MIST	15.20	15.13	172.70	178.79	0.3320	0.3362	0.6325	0.6321	0.0914	0.0919
	SDS	<u>16.83</u>	<u>16.79</u>	<u>167.93</u>	<u>167.95</u>	0.2930	0.2898	<u>0.5755</u>	<u>0.5737</u>	<u>0.0560</u>	<u>0.0560</u>
	Ours-	14.94	15.00	209.43	208.02	0.2939	0.2909	0.6859	0.6861	0.1136	0.1129
	Ours+	<b>18.55</b>	<b>18.58</b>	<b>114.34</b>	<b>112.30</b>	<b>0.4348</b>	<b>0.4355</b>	<b>0.5420</b>	<b>0.5405</b>	0.0605	0.0605
P4	clean	18.82	18.84	69.26	69.17	0.5886	0.5905	0.4116	0.4096	0.0256	0.0256
	AdvDM	16.65	16.62	165.67	<u>162.57</u>	0.2730	0.2712	0.5911	0.5898	<b>0.0567</b>	<b>0.0564</b>
	PG	15.81	15.83	175.06	172.92	<u>0.3312</u>	<u>0.3370</u>	0.6364	0.6350	0.0880	0.0893
	MIST	15.76	15.78	175.06	173.78	0.3241	0.3281	0.6348	0.6335	0.0847	0.0863
	SDS	<u>16.87</u>	<u>16.85</u>	<u>165.40</u>	164.08	0.2944	0.2913	0.5798	0.5786	<u>0.0590</u>	<u>0.0587</u>
	Ours-	16.17	16.10	136.47	136.37	0.3440	0.3306	0.6704	0.6744	0.1094	0.1108
	Ours+	<b>18.72</b>	<b>18.77</b>	<b>110.03</b>	<b>109.44</b>	<b>0.4447</b>	<b>0.4447</b>	<b>0.5396</b>	<b>0.5385</b>	0.0614	0.0609
P5	clean	18.52	18.55	83.84	82.33	0.5724	0.5737	0.4321	0.4298	0.0268	0.0267
	AdvDM	16.54	16.47	180.73	181.80	0.2609	0.2592	0.5925	0.5923	<b>0.0559</b>	<b>0.0553</b>
	PG	15.70	15.70	160.79	157.27	<u>0.3655</u>	<u>0.3537</u>	0.6209	0.6231	0.1001	0.0982
	MIST	15.67	15.66	<u>157.99</u>	<u>156.52</u>	0.3606	0.3471	0.6179	0.6201	0.0974	0.0955
	SDS	<u>16.73</u>	<u>16.61</u>	182.40	183.48	0.2769	0.2734	0.5855	<u>0.5860</u>	<u>0.0588</u>	<u>0.0585</u>
	Ours-	15.17	15.28	182.18	174.89	0.3422	0.3363	0.6783	0.6776	0.1241	0.1228
	Ours+	<b>18.50</b>	<b>18.40</b>	<b>124.06</b>	<b>127.72</b>	<b>0.4144</b>	<b>0.4092</b>	<b>0.5441</b>	<b>0.5444</b>	0.0618	0.0640

Table 2: Results on IQAs taken between the clean image  $x$  and the adversarial sample after editing  $f(x_{adv})$ . In this table, the better IQAs representing the better performance. Notbaly, “clean” for each prompt is the IQA computed between clean image  $x$  and edited clean image  $f(x)$ .

prompt	method	PSNR $\uparrow$		FID $\downarrow$		SSIM $\uparrow$		LPIPS $\downarrow$		ACDM $\downarrow$	
		SD14	SD15	SD14	SD15	SD14	SD15	SD14	SD15	SD14	SD15
P1	AdvDM	20.49	20.49	<u>153.71</u>	<u>150.22</u>	<b>0.4422</b>	<b>0.4417</b>	0.5010	0.5008	0.0416	0.0424
	PG	<u>18.49</u>	<u>18.52</u>	151.75	147.85	0.4800	0.4840	<u>0.5647</u>	<u>0.5629</u>	<u>0.0786</u>	<u>0.0792</u>
	MIST	18.50	18.54	150.20	147.78	0.4759	0.4797	0.5604	0.5585	0.0751	0.0757
	SDS	20.60	20.56	<b>155.55</b>	<b>152.76</b>	0.4519	0.4495	0.4998	0.5007	0.0453	0.0462
	Ours-	<b>18.02</b>	<b>18.02</b>	139.11	135.32	<u>0.4441</u>	<u>0.4453</u>	<b>0.6188</b>	<b>0.6171</b>	<b>0.1106</b>	<b>0.1110</b>
	Ours+	22.08	22.05	91.43	91.19	0.5744	0.5736	0.4747	0.4738	0.0551	0.0560
P2	AdvDM	19.23	19.25	94.90	<u>92.09</u>	<b>0.4226</b>	<b>0.4232</b>	0.5017	0.5001	0.0442	0.0440
	PG	<u>17.32</u>	<u>17.31</u>	88.43	91.00	0.4650	0.4660	<u>0.5585</u>	<u>0.5592</u>	<u>0.0858</u>	<u>0.0865</u>
	MIST	<u>17.32</u>	17.32	88.17	88.87	0.4616	0.4632	0.5539	0.5552	0.0830	0.0837
	SDS	19.32	19.31	<b>99.80</b>	<b>99.03</b>	<u>0.4312</u>	<u>0.4304</u>	0.5035	0.5029	0.0480	0.0483
	Ours-	<b>16.74</b>	<b>16.70</b>	70.59	69.04	0.4336	0.4329	<b>0.6005</b>	<b>0.5990</b>	<b>0.1156</b>	<b>0.1167</b>
	Ours+	20.70	20.69	64.27	64.44	0.5524	0.5518	0.4789	0.4786	0.0550	0.0558
P3	AdvDM	19.37	19.42	143.57	140.01	<u>0.4291</u>	0.4298	0.5142	0.5102	0.0454	0.0452
	PG	<u>17.26</u>	17.22	123.94	127.87	0.4702	0.4749	<u>0.5727</u>	<u>0.5727</u>	<u>0.0847</u>	<u>0.0853</u>
	MIST	17.27	<u>17.18</u>	121.36	127.34	0.4685	0.4732	0.5691	0.5687	0.0820	0.0829
	SDS	19.56	19.59	<u>144.63</u>	<u>144.64</u>	0.4409	0.4385	0.5128	0.5102	0.0492	0.0491
	Ours-	<b>16.71</b>	<b>16.78</b>	<b>156.47</b>	<b>153.85</b>	<b>0.4234</b>	<b>0.4228</b>	<b>0.6202</b>	<b>0.6204</b>	<b>0.1084</b>	<b>0.1079</b>
	Ours+	20.82	20.89	87.04	85.61	0.5554	0.5568	0.4878	0.4868	0.0571	0.0571
P4	AdvDM	19.32	19.31	148.26	145.27	<u>0.4045</u>	0.4040	0.5347	0.5324	0.0488	0.0486
	PG	<u>17.87</u>	<u>17.84</u>	<b>150.85</b>	<b>151.75</b>	0.4560	0.4589	0.5820	0.5818	0.0804	0.0819
	MIST	17.88	17.85	148.64	<u>150.45</u>	0.4526	0.4540	0.5786	0.5788	0.0770	0.0786
	SDS	19.49	19.48	<u>149.37</u>	148.82	0.4196	0.4176	0.5293	0.5275	0.0522	0.0520
	Ours-	<b>17.61</b>	<b>17.50</b>	116.48	115.41	<b>0.4004</b>	<b>0.3942</b>	<b>0.6361</b>	<b>0.6394</b>	<b>0.1051</b>	<b>0.1067</b>
	Ours+	21.24	21.31	90.18	89.56	0.5553	0.5572	0.4921	0.4903	0.0558	0.0556
P5	AdvDM	19.41	19.33	<u>159.45</u>	<u>166.76</u>	<b>0.4088</b>	<b>0.4076</b>	0.5239	0.5226	0.0445	0.0441
	PG	<u>17.77</u>	<u>17.80</u>	110.96	112.49	0.5091	0.4988	0.5460	<u>0.5517</u>	<u>0.0945</u>	<u>0.0924</u>
	MIST	17.81	17.82	107.88	110.79	0.5087	0.4972	0.5404	0.5459	0.0915	0.0892
	SDS	19.48	19.39	<b>162.63</b>	<b>170.77</b>	<u>0.4171</u>	<u>0.4149</u>	0.5239	0.5236	0.0487	0.0485
	Ours-	<b>16.81</b>	<b>16.95</b>	134.71	129.93	0.4568	0.4524	<b>0.6032</b>	<b>0.6047</b>	<b>0.1227</b>	<b>0.1209</b>
	Ours+	21.00	20.92	99.70	106.53	0.5402	0.5357	0.4857	0.4867	0.0548	0.0573

Table 3: Results on IQAs taken between the clean image after editing  $f(x)$  and the adversarial sample after editing  $f(x_{adv})$ . In this table, the worse IQAs representing the better performance.



Figure 6: A visualization with P1 = “”, P2 = “a fresh ripe pineapple is on the stem”, P3 = “add some snow”, P4 = “apply sunset lighting”, P5 = “make it like a watercolor painting”.

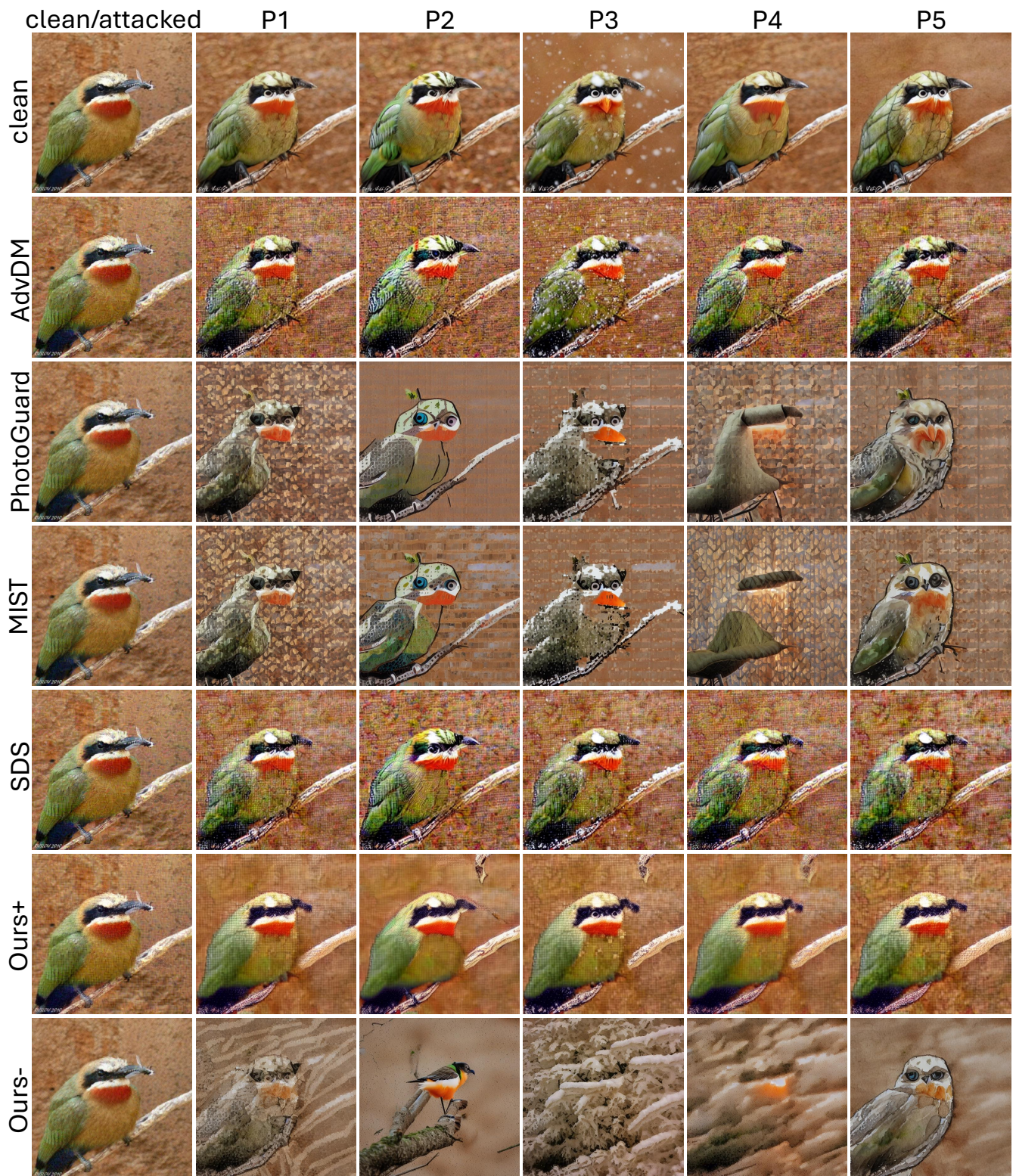


Figure 7: A visualization with P1 = “”, P2 = “a colorful bird is perched on a tree branch”, P3 = “add some snow”, P4 = “apply sunset lighting”, P5 = “make it like a watercolor painting”.



## Ablation Studies and Extra Evaluations

We conduct comprehensive ablation studies on all hyperparameters. It is worth noting that, all metrics taken in the ablation is following the form of PCA- (Objective 2). For the hyperparameter  $v$ , we also do the ablation with evaluating metrics following the form of PCA+ (Objective 1), which aims to evidence our choice of  $\mathcal{N}(\mathbf{0}, \mathbf{I})$  for PCA+ and  $\mathcal{N}(\mathbf{0}, \mathbf{0})$  for PCA-

### Ablation on $v$

We conduct an ablation study on the variance hyperparameter  $v$  in our attack target distribution  $p^*(z) = \mathcal{N}(\mathbf{0}, v\mathbf{I})$ . This hyperparameter controls the extent of the latent space manipulation in our attack.

We compare two values,  $v = 1$  and  $v = 1 \times 10^{-8}$ , for both PCA+ and PCA- methods. The choice of  $v = 10^{-8}$  is to approximate a variance close to 0 while maintaining numerical stability.

**PCA+** For PCA+, our objective is to maintain consistency with the original image while still preventing unauthorized edits. As shown in Table 4, the performance of PCA+ is remarkably similar for both  $v = 1$  and  $v = 1 \times 10^{-8}$  across most metrics.

prompt	v	PSNR $\uparrow$		FID $\downarrow$		SSIM $\uparrow$		LPIPS $\downarrow$		ACDM $\downarrow$	
		SD14	SD15	SD14	SD15	SD14	SD15	SD14	SD15	SD14	SD15
P1	clean	19.09	19.09	54.95	54.25	0.5911	0.5914	0.3948	0.3943	0.0243	0.0242
	1	18.85	18.82	109.01	108.57	0.4424	0.4396	0.5349	0.5345	0.0593	0.0601
	1e-8	18.86	18.83	112.57	111.86	0.4512	0.4475	0.5286	0.5285	0.0582	0.0588
P2	clean	18.68	18.69	45.34	45.41	0.5829	0.5838	0.3993	0.3986	0.0253	0.0251
	1	18.61	18.60	70.40	70.08	0.4460	0.4444	0.5276	0.5269	0.0602	0.0608
	1e-8	18.62	18.60	72.28	73.06	0.4563	0.4535	0.5202	0.5204	0.0590	0.0596
P3	clean	18.50	18.54	78.89	78.98	0.5722	0.5735	0.4284	0.4281	0.0268	0.0266
	1	18.55	18.58	114.34	112.30	0.4348	0.4355	0.5420	0.5405	0.0605	0.0605
	1e-8	18.59	18.64	116.97	116.55	0.4442	0.4437	0.5348	0.5334	0.0591	0.0592
P4	clean	18.82	18.84	69.26	69.17	0.5886	0.5905	0.4116	0.4096	0.0256	0.0256
	1	18.72	18.77	110.03	109.44	0.4447	0.4447	0.5396	0.5385	0.0614	0.0609
	1e-8	18.72	18.76	114.24	112.44	0.4539	0.4523	0.5329	0.5324	0.0606	0.0603
P5	clean	18.52	18.55	83.84	82.33	0.5724	0.5737	0.4321	0.4298	0.0268	0.0267
	1	18.50	18.40	124.06	127.72	0.4144	0.4092	0.5441	0.5444	0.0618	0.0640
	1e-8	18.50	18.39	129.09	130.72	0.4233	0.4173	0.5395	0.5401	0.0612	0.0632

Table 4: Ablation study on  $v$ . In this table, IQAs are taken between the clean image  $x$  and the adversarial sample after editing  $f(x_{adv})$ . The better IQAs representing the better performance. Notbaly, “clean” for each prompt is the IQA computed between clean image  $x$  and edited clean image  $f(x)$ .

Analyzing the results, we observe that the performance metrics for  $v = 1$  and  $v = 1 \times 10^{-8}$  are nearly identical in most cases. This similarity suggests that both values of  $v$  are capable of achieving the primary goal of PCA+, which is to preserve the original image characteristics while preventing unauthorized edits.

However, a closer examination reveals a subtle but important difference: the FID scores for  $v = 1$  are consistently slightly lower across all prompts and models. This lower FID indicates that images generated with  $v = 1$  are marginally closer to the distribution of real images, representing a slightly better preservation of overall image quality and realism.

The marginally superior FID performance of  $v = 1$  can be attributed to its alignment with the standard normal distribution, which is commonly used as the prior in many diffusion models. This alignment allows for a more natural manipulation of the latent space, resulting in outputs that are subtly more consistent with the expected image distribution.

Based on this observation, we choose  $v = 1$  for our main experiments with PCA+. While the differences are small, the consistently lower FID scores for  $v = 1$  suggest a slight advantage in maintaining image realism. This choice allows us to optimally balance our dual objectives of preserving image quality and preventing unauthorized edits, making it the preferred setting for our PCA+ method.

**PCA-** As shown in Table 5, setting  $v$  close to 0 outperforms  $v = 1$  across all prompts and both models, as evidenced by all five evaluated metrics. For instance, with prompt P1 on SD14, when  $v$  decreases from 1 to 1e-8, PSNR decreases from 18.65 to 18.02, FID increases from 124.33 to 139.11, and SSIM increases from 0.4299 to 0.4441, all indicating enhanced attack effectiveness. This consistent improvement can be attributed to the tighter concentration of the target distribution around zero when  $v$  is smaller. A smaller  $v$  encourages the posterior distribution to collapse more severely, leading to more significant disruption in the latent space and, consequently, in the generated images. Our choice of  $v = 1e - 8$  in the main experiments reflects this finding, providing a balance between strong attack performance and numerical stability. This ablation study further demonstrates the flexibility of our method and the importance of carefully tuning hyperparameters for optimal performance.

prompt	$v$	PSNR $\uparrow$		FID $\downarrow$		SSIM $\uparrow$		LPIPS $\downarrow$		ACDM $\downarrow$	
		SD14	SD15	SD14	SD15	SD14	SD15	SD14	SD15	SD14	SD15
P1	1	18.65	18.65	124.33	124.37	0.4299	0.4317	0.5932	0.5927	0.0838	0.0844
	1e-8	<b>18.02</b>	<b>18.02</b>	<b>139.11</b>	<b>135.32</b>	<b>0.4441</b>	<b>0.4453</b>	<b>0.6188</b>	<b>0.6171</b>	<b>0.1106</b>	<b>0.1110</b>
P2	1	17.34	17.31	63.33	62.23	0.4251	0.4244	0.5768	0.5758	0.0897	0.0898
	1e-8	<b>16.74</b>	<b>16.70</b>	<b>70.59</b>	<b>69.04</b>	<b>0.4336</b>	<b>0.4329</b>	<b>0.6005</b>	<b>0.5990</b>	<b>0.1156</b>	<b>0.1167</b>
P3	1	17.12	17.15	128.91	128.16	0.4108	0.4100	0.6024	0.6027	0.0856	0.0851
	1e-8	<b>16.71</b>	<b>16.78</b>	<b>156.47</b>	<b>153.85</b>	<b>0.4234</b>	<b>0.4228</b>	<b>0.6202</b>	<b>0.6204</b>	<b>0.1084</b>	<b>0.1079</b>
P4	1	18.08	18.00	106.21	103.85	0.3768	0.3745	0.6305	0.6325	0.0784	0.0787
	1e-8	<b>17.61</b>	<b>17.50</b>	<b>116.48</b>	<b>115.41</b>	<b>0.4004</b>	<b>0.3942</b>	<b>0.6361</b>	<b>0.6394</b>	<b>0.1051</b>	<b>0.1067</b>
P5	1	17.44	17.59	120.47	116.90	0.4491	0.4436	0.5871	0.5888	0.0957	0.0939
	1e-8	<b>16.81</b>	<b>16.95</b>	<b>134.71</b>	<b>129.93</b>	<b>0.4568</b>	<b>0.4524</b>	<b>0.6032</b>	<b>0.6047</b>	<b>0.1227</b>	<b>0.1209</b>

Table 5: Ablation study on  $v$ . In this table, IQAs are taken between the clean image after editing  $f(x)$  and the adversarial sample after editing  $f(x_{adv})$ . The worse IQAs representing the better performance.

### Ablation on different surrogate VAE

We conducted an ablation study to investigate the impact of using different VAEs as surrogate models in our attack. We compared the performance of VAEs from SD14 and SD15 across five different prompts (P1 to P5) and evaluated their effectiveness on both SD14 and SD15 models. Table 6 presents the results of this study.

prompt	VAE	PSNR $\uparrow$		FID $\downarrow$		SSIM $\uparrow$		LPIPS $\downarrow$		ACDM $\downarrow$	
		SD14	SD15	SD14	SD15	SD14	SD15	SD14	SD15	SD14	SD15
P1	SD14	18.02	18.02	139.57	136.62	0.4438	0.4454	0.6186	0.6170	0.1105	0.1111
	SD15	18.02	18.02	139.11	135.32	0.4441	0.4453	0.6188	0.6171	0.1106	0.1110
P2	SD14	16.74	16.70	72.01	69.71	0.4348	0.4338	0.5998	0.5986	0.1161	0.1169
	SD15	16.74	16.70	70.59	69.04	0.4336	0.4329	0.6005	0.5990	0.1156	0.1167
P3	SD14	16.71	16.78	154.99	153.13	0.4226	0.4232	0.6205	0.6206	0.1077	0.1083
	SD15	16.71	16.78	156.47	153.85	0.4234	0.4228	0.6202	0.6204	0.1084	0.1079
P4	SD14	17.61	17.49	118.64	115.96	0.3994	0.3931	0.6363	0.6395	0.1051	0.1063
	SD15	17.61	17.50	116.48	115.41	0.4004	0.3942	0.6361	0.6394	0.1051	0.1067
P5	SD14	16.81	16.94	134.53	130.34	0.4574	0.4523	0.6032	0.6048	0.1228	0.1205
	SD15	16.81	16.95	134.71	129.93	0.4568	0.4524	0.6032	0.6047	0.1227	0.1209

Table 6: Ablation study on different VAEs.

The results show that the choice of surrogate VAE has minimal impact on the attack performance. For most prompts and metrics, the differences between using SD14 VAE and SD15 VAE are negligible. For example, with prompt P1 on SD14, the PSNR values are identical (18.02) for both VAEs, and other metrics show only slight variations.

This consistency across different VAEs suggests that our attack method is robust to the choice of surrogate model. It demonstrates that the vulnerabilities we exploit are inherent to the VAE structure rather than specific to a particular model implementation. This finding has important implications for the generalizability of our attack, as it indicates that an attacker does not need access to the exact VAE used in the target model to mount an effective attack.

The robustness to surrogate model choice further supports the practical applicability of our method, as it can potentially be effective against a wide range of LDM implementations using only publicly available VAE models.

### Ablation on $\alpha$

We conducted an ablation study on the learning rate  $\alpha$  used in our projected sign gradient ascent. We experimented with  $\alpha$  values of 1, 2, and 4 across five different prompts (P1 to P5) and two Stable Diffusion models (SD14 and SD15). Table 7 presents the results of this study.

As shown in Table 7,  $\alpha = 2$  generally yields the best performance across most prompts and metrics. For example, with prompt P1 on SD14, when  $\alpha = 2$ , we observe the lowest PSNR (18.02), highest FID (139.11), and highest ACDM (0.1106), indicating the most effective attack. This trend is consistent across different prompts and both models, with a few exceptions where  $\alpha = 1$  or  $\alpha = 4$  perform slightly better in specific metrics.

The superior performance of  $\alpha = 2$  suggests that this learning rate provides an optimal balance between the step size and the number of iterations in our attack algorithm. It allows for sufficiently large updates to effectively perturb the latent space while avoiding overshooting that might occur with larger learning rates.

prompt	$\alpha$	PSNR $\uparrow$		FID $\downarrow$		SSIM $\uparrow$		LPIPS $\downarrow$		ACDM $\downarrow$	
		SD14	SD15	SD14	SD15	SD14	SD15	SD14	SD15	SD14	SD15
P1	1	18.18	18.18	137.44	134.12	0.4563	0.4576	0.6137	0.6119	0.1075	0.1080
	2	<b>18.02</b>	<b>18.02</b>	<b>139.11</b>	<b>135.32</b>	0.4441	0.4453	<b>0.6188</b>	<b>0.6171</b>	<b>0.1106</b>	<b>0.1110</b>
	4	18.43	18.44	132.79	132.77	<b>0.4408</b>	<b>0.4419</b>	0.6057	0.6049	0.0961	0.0966
P2	1	16.85	16.82	70.40	68.52	0.4448	0.4445	0.5956	0.5938	0.1131	0.1142
	2	<b>16.74</b>	<b>16.70</b>	<b>70.59</b>	<b>69.04</b>	0.4336	0.4329	<b>0.6005</b>	<b>0.5990</b>	<b>0.1156</b>	<b>0.1167</b>
	4	17.10	17.08	66.88	65.54	<b>0.4330</b>	<b>0.4327</b>	0.5887	0.5863	0.1018	0.1026
P3	1	16.86	16.91	155.70	152.69	0.4330	0.4323	0.6165	0.6171	0.1052	0.1053
	2	<b>16.71</b>	<b>16.78</b>	<b>156.47</b>	<b>153.85</b>	0.4234	0.4228	<b>0.6202</b>	<b>0.6204</b>	<b>0.1084</b>	<b>0.1079</b>
	4	17.00	17.04	140.65	139.28	<b>0.4198</b>	<b>0.4189</b>	0.6110	0.6108	0.0958	0.0956
P4	1	17.75	17.62	<b>118.34</b>	113.48	0.4138	0.4067	0.6305	0.6337	0.1021	0.1036
	2	<b>17.61</b>	<b>17.50</b>	116.48	<b>115.41</b>	0.4004	0.3942	<b>0.6361</b>	<b>0.6394</b>	<b>0.1051</b>	<b>0.1067</b>
	4	17.96	17.85	110.58	109.59	<b>0.3929</b>	<b>0.3876</b>	0.6302	0.6347	0.0918	0.0927
P5	1	16.91	17.06	132.37	128.71	0.4670	0.4628	0.5989	0.6004	0.1207	0.1182
	2	<b>16.81</b>	<b>16.95</b>	<b>134.71</b>	<b>129.93</b>	0.4568	0.4524	<b>0.6032</b>	<b>0.6047</b>	<b>0.1227</b>	<b>0.1209</b>
	4	17.18	17.33	126.82	124.19	<b>0.4547</b>	<b>0.4516</b>	0.5932	0.5939	0.1088	0.1073

Table 7: Ablation study on  $\alpha$ .

This ablation study demonstrates the importance of carefully tuning the learning rate in our attack method and justifies our choice of  $\alpha = 2$  in the main experiments.

#### Ablation on $t$

To investigate the impact of the number of attack steps on our method’s performance, we conducted an ablation study varying the attack steps  $T$ . We experimented with  $T$  values of 10, 20, and 40 across five different prompts (P1 to P5) and two Stable Diffusion models (SD14 and SD15). Table 8 presents the results of this study.

prompt	$T$	PSNR $\uparrow$		FID $\downarrow$		SSIM $\uparrow$		LPIPS $\downarrow$		ACDM $\downarrow$	
		SD14	SD15	SD14	SD15	SD14	SD15	SD14	SD15	SD14	SD15
P1	10	19.25	19.26	120.48	117.95	0.4768	0.4781	0.5735	0.5732	0.0732	0.0735
	20	18.52	18.52	132.32	129.64	0.4512	0.4525	0.6013	0.6006	0.0941	0.0945
	40	<b>18.02</b>	<b>18.02</b>	<b>139.11</b>	<b>135.32</b>	<b>0.4441</b>	<b>0.4453</b>	<b>0.6188</b>	<b>0.6171</b>	<b>0.1106</b>	<b>0.1110</b>
P2	10	17.77	17.74	61.98	61.11	0.4664	0.4657	0.5561	0.5533	0.0812	0.0819
	20	17.17	17.12	67.02	65.80	0.4435	0.4421	0.5825	0.5813	0.1005	0.1010
	40	<b>16.74</b>	<b>16.70</b>	<b>70.59</b>	<b>69.04</b>	<b>0.4336</b>	<b>0.4329</b>	<b>0.6005</b>	<b>0.5990</b>	<b>0.1156</b>	<b>0.1167</b>
P3	10	17.66	17.70	124.79	123.90	0.4490	0.4498	0.5853	0.5853	0.0759	0.0764
	20	17.09	17.14	138.87	140.27	0.4296	0.4292	0.6065	0.6065	0.0938	0.0941
	40	<b>16.71</b>	<b>16.78</b>	<b>156.47</b>	<b>153.85</b>	<b>0.4234</b>	<b>0.4228</b>	<b>0.6202</b>	<b>0.6204</b>	<b>0.1084</b>	<b>0.1079</b>
P4	10	18.66	18.55	102.88	100.43	0.4325	0.4273	0.6020	0.6058	0.0700	0.0707
	20	18.03	17.91	111.28	108.82	0.4060	0.4010	0.6232	0.6269	0.0896	0.0908
	40	<b>17.61</b>	<b>17.50</b>	<b>116.48</b>	<b>115.41</b>	<b>0.4004</b>	<b>0.3942</b>	<b>0.6361</b>	<b>0.6394</b>	<b>0.1051</b>	<b>0.1067</b>
P5	10	17.77	17.94	112.76	111.11	0.4880	0.4850	0.5619	0.5634	0.0904	0.0886
	20	17.20	17.36	125.51	122.68	0.4659	0.4616	0.5868	0.5884	0.1083	0.1065
	40	<b>16.81</b>	<b>16.95</b>	<b>134.71</b>	<b>129.93</b>	<b>0.4568</b>	<b>0.4524</b>	<b>0.6032</b>	<b>0.6047</b>	<b>0.1227</b>	<b>0.1209</b>

Table 8: Ablation study on  $t$ .

As shown in Table 8, the performance of our method consistently improves as the number of attack steps increases across all prompts and both models. This trend is evident in all five evaluated metrics: PSNR, FID, SSIM, LPIPS, and ACDM. For example, with prompt P1 on SD14, as  $t$  increases from 10 to 40, PSNR decreases from 19.25 to 18.02, FID increases from 120.48 to 139.11, and SSIM decreases from 0.4768 to 0.4441, all indicating enhanced attack effectiveness.

This consistent pattern suggests a strong positive correlation between the number of attack steps and the effectiveness of our Posterior Collapse Attack. The improvement can be attributed to the iterative nature of our approach, allowing for finer-grained adjustments to the adversarial perturbation with each step. Our choice of  $T = 40$  in the main experiments represents a balance between attack effectiveness and computational efficiency.

## Detailed Analysis of VAE Reconstruction Quality

Table 9 presents a comprehensive comparison of IQAs for VAE reconstructions of adversarial samples generated by different methods. The top row ( $x^{\text{recon}}$ ) shows the baseline IQA values for reconstructions of clean images, providing a reference point for the effectiveness of each attack method.

Methods	IQAs				
	PSNR $\uparrow$	FID $\downarrow$	SSIM $\uparrow$	LPIPS $\downarrow$	ACDM $\downarrow$
$x^{\text{recon}}$	29.11	3.73	0.8683	0.1022	0.0286
AdvDM	24.50	28.02	0.5916	0.4500	0.0384
PG	<u>22.67</u>	<u>63.56</u>	0.5740	<u>0.5550</u>	<u>0.0716</u>
$x^{\text{adv}}$ MIST	22.70	62.27	<u>0.5668</u>	0.5545	0.0699
SDS	24.27	25.99	0.6038	0.4322	0.0413
Ours	<b>21.64</b>	<b>72.54</b>	<b>0.5461</b>	<b>0.5838</b>	<b>0.0886</b>

Table 9: Comparison of IQAs for VAE reconstructions of adversarial samples across different methods.

Our proposed Posterior Collapse Attack demonstrates superior performance across all five IQA metrics when considering the reconstructed adversarial samples ( $x^{\text{adv}}$ ). Specifically, our method achieves the lowest PSNR (21.64) and SSIM (0.5461) scores, indicating the most significant degradation in structural similarity between the original and reconstructed adversarial images. The highest FID score (72.54) further corroborates that our method produces reconstructions that deviate substantially from the original image distribution. Moreover, our approach yields the highest LPIPS (0.5838) and ACDM (0.0886) scores, suggesting greater perceptual differences and color discrepancies in the reconstructed adversarial samples. These results consistently outperform other baseline methods.

Our method consistently outperforms other baselines across all IQA metrics, notably without access to the VAE decoder parameters. This constraint makes our approach more realistic and challenging. The significant changes in PSNR, SSIM, FID, LPIPS, and ACDM scores of the reconstructed images demonstrate our method’s effectiveness in inducing substantial distortions in the latent space, which persist through the decoding process. By achieving such disruption without decoder access, our Posterior Collapse Attack presents a practical approach to protecting against unauthorized image manipulation in real-world scenarios where full model access is often unavailable.

## Runtime across Different Resolutions

Table 10 presents the runtime and VRAM usage of our proposed method across different image resolutions. These measurements were conducted under the same testing environment as the results presented in Figure 1 of the main paper, using the setup provided by SDS<sup>2</sup>. All experiments were performed on a single consumer-grade NVIDIA RTX 3090 GPU. Consistent with the

resolution	runtime	VRAM
256	1.6	3.4G
512	5.9	6.7G
1024	24.7	22.3G

Table 10: Runtime of our proposed method across different resolutions.

main paper, we set the number of iterations  $t$  to 40 and the variance  $v$  to  $1e-8$ . This consistency in both hardware and hyperparameters eliminates potential variations in runtime due to differences in setup, CUDA versions, or library implementations.

Our method demonstrates efficient performance across various resolutions. For 256x256 images, it requires only 1.6 seconds and 3.4GB of VRAM, scaling up to 24.7 seconds and 22.3GB for 1024x1024 images. The use of an RTX 3090, a common high-end consumer GPU, ensures that these results are representative of real-world performance for many users.

The sub-linear increase in runtime relative to the quadratic increase in pixel count (from 256 to 1024, a 16-fold increase in pixels) indicates good algorithmic efficiency. This performance profile, coupled with the accessibility of the testing hardware, suggests that our approach is practical for a wide range of applications and users, from processing smaller images on modest systems to handling high-resolution images on more powerful setups.

<sup>2</sup><https://github.com/xavihart/Diff-Protect>

## Implementation Details

Our proposed method is implemented using PyTorch (Paszke et al. 2019) and the Diffusers library (von Platen et al. 2022). We maintain consistency across all experiments by fixing the random seed to 3407 for PyTorch’s generator (Picard 2021), ensuring reproducibility in all stable diffusion image generations.

### Latent Diffusion Models

We utilize two LDMs in our experiments: SD14<sup>3</sup> and SD15<sup>4</sup> as victim model. To test the transferability of our method and baselines, we also utilize the SDXL<sup>5</sup> and SD20<sup>6</sup>. Unless specifically mentioned in the main paper, all inference parameters for these models are set to their default values.

### Image Quality Assessment Metrics

We employ five IQA metrics in our evaluation:

- PSNR: Range set to 1, aligning with PyTorch’s image transformation.
- FID: Implemented using TorchEval<sup>7</sup> with default settings.
- SSIM<sup>8</sup>: Gaussian kernel size set to 11.
- LPIPS<sup>9</sup>: Utilizing VGG (Simonyan and Zisserman 2015) as the surrogate model.
- ACDM<sup>10</sup>: Gaussian kernel size set to 11.

### Baseline Methods

For comparative analysis, we follow the implementation of SDS<sup>2</sup>. To ensure fair comparison, we maintain all default parameters except for the attack time step, which is set to 40 across all methods.

### Hardware and Environment

The majority of our experiments were conducted on two separate NVIDIA A100-SXM4-80GB GPUs. For transparency and reproducibility, we craft a Docker image based on the diffusers’ official docker<sup>11</sup> for the whole project, unless mentioned, all experiments are done in those two machines with the same Docker image.

---

<sup>3</sup><https://huggingface.co/CompVis/stable-diffusion-v1-4>

<sup>4</sup><https://huggingface.co/runwayml/stable-diffusion-v1-5>

<sup>5</sup><https://huggingface.co/stabilityai/stable-diffusion-xl-base-1.0>

<sup>6</sup>[stabilityai/stable-diffusion-2](https://stabilityai/stable-diffusion-2)

<sup>7</sup><https://pytorch.org/torcheval/stable/>

<sup>8</sup><https://github.com/Po-Hsun-Su/pytorch-ssim>

<sup>9</sup><https://github.com/richzhang/PerceptualSimilarity>

<sup>10</sup><https://github.com/ZhongliangGuo/ACDM>

<sup>11</sup><https://hub.docker.com/r/diffusers/diffusers-pytorch-xformers-cuda>